



## Estimates of mass absorption cross sections of black carbon for filter-based absorption photometers in the Arctic

Sho Ohata<sup>1,2,\*</sup>, Tatsuhiro Mori<sup>3,4,\*</sup>, Yutaka Kondo<sup>5,\*</sup>, Sangeeta Sharma<sup>6</sup>, Antti Hyvärinen<sup>7</sup>, Elisabeth  
5 Andrews<sup>8,9</sup>, Peter Tunved<sup>10</sup>, Eija Asmi<sup>7</sup>, John Backman<sup>7</sup>, Henri Servomaa<sup>7</sup>, Daniel Veber<sup>6</sup>,  
Konstantinos Eleftheriadis<sup>11</sup>, Stergios Vratolis<sup>11</sup>, Makoto Koike<sup>3</sup>, Yugo Kanaya<sup>12,13</sup>, Atsushi Yoshida<sup>5</sup>,  
Nobuhiro Moteki<sup>3</sup>, Yongjing Zhao<sup>14</sup>, Yutaka Tobo<sup>5,15</sup>, Junji Matsushita<sup>5</sup>, and Naga Oshima<sup>16</sup>

- <sup>1</sup>Institute for Space–Earth Environmental Research, Nagoya University, Nagoya, Aichi, Japan  
10 <sup>2</sup>Institute for Advanced Research, Nagoya University, Nagoya, Aichi, Japan  
<sup>3</sup>Department of Earth and Planetary Science, Graduate School of Science, The University of Tokyo, Tokyo, Japan  
<sup>4</sup>Department of Physics, Faculty of Science Division I, Tokyo University of Science, Tokyo, Japan  
<sup>5</sup>National Institute of Polar Research, Tachikawa, Tokyo, Japan  
15 <sup>6</sup>Climate Chemistry Measurements Research/Climate Research Division, Environment and Climate Change Canada/Government of Canada  
<sup>7</sup>Finnish Meteorological Institute, Helsinki, Finland  
<sup>8</sup>Cooperative Institute for Research in Environmental Sciences (CIRES), University of Colorado, Boulder, CO, USA  
20 <sup>9</sup>NOAA Global Monitoring Laboratory, 325 Broadway, Boulder, CO, USA  
<sup>10</sup>Department of Environmental Science and Analytical Chemistry (ACES), Atmospheric Science Unit, Stockholm University, Stockholm, Sweden  
<sup>11</sup>Environmental Radioactivity Laboratory (ERL), Institute of Nuclear and Radiological Science & Technology, Energy & Safety, National Centre for Scientific Research “Demokritos”, 15310 Attiki, Greece  
25 <sup>12</sup>Research Institute for Global Change (RIGC), Japan Agency for Marine–Earth Science and Technology (JAMSTEC), Yokohama, Kanagawa, Japan  
<sup>13</sup>Graduate School of Maritime Sciences, Kobe University, Kobe, Japan  
<sup>14</sup>Air Quality Research Center, University of California, Davis, CA, USA  
<sup>15</sup>Department of Polar Science, School of Multidisciplinary Sciences, The Graduate University for Advanced  
30 Studies, SOKENDAI, Tachikawa, Tokyo, Japan  
<sup>16</sup>Meteorological Research Institute, Tsukuba, Japan

\*These authors contributed equally to this work.

35 *Correspondence to:* Sho Ohata (sho.ohata@isee.nagoya-u.ac.jp)

Running title: Normalization of BC measurements by COSMOS



**Abstract.** Long-term measurements of atmospheric mass concentrations of black carbon (BC) are  
40 needed to investigate changes in its emission, transport, and deposition. However, depending on  
instrumentation, parameters related to BC such as aerosol absorption coefficient ( $b_{\text{abs}}$ ) have been  
measured instead. Most ground-based measurements of  $b_{\text{abs}}$  in the Arctic have been made by filter-  
based absorption photometers, including particle soot absorption photometers (PSAP), continuous light  
absorption photometer (CLAP), Aethalometers, and multi-angle absorption photometers (MAAP). The  
45 measured  $b_{\text{abs}}$  can be converted to mass concentrations of BC ( $M_{\text{BC}}$ ) by assuming the value of the mass  
absorption cross section (MAC;  $M_{\text{BC}} = b_{\text{abs}}/\text{MAC}$ ). However, the accuracy of conversion of  $b_{\text{abs}}$  to  $M_{\text{BC}}$   
has not been adequately assessed. Here, we introduce a systematic method for deriving MAC values  
from  $b_{\text{abs}}$  measured by these instruments and independently measured  $M_{\text{BC}}$ . In this method,  $M_{\text{BC}}$  was  
measured with a filter-based absorption photometer with a heated inlet (COSMOS). COSMOS-derived  
50  $M_{\text{BC}}$  ( $M_{\text{BC}}$  (COSMOS)) is traceable to a rigorously calibrated single particle soot photometer (SP2) and  
the absolute accuracy of  $M_{\text{BC}}$  (COSMOS) has been demonstrated previously to be about 15 % in Asia  
and the Arctic. The necessary conditions for application of this method are a high correlation of the  
measured  $b_{\text{abs}}$  with independently measured  $M_{\text{BC}}$ , and long-term stability of the regression slope, which  
is denoted as  $\text{MAC}_{\text{cor}}$  (MAC derived from the correlation). In general,  $b_{\text{abs}}-M_{\text{BC}}$  (COSMOS)  
55 correlations were high ( $r^2 = 0.76-0.95$  for hourly data) at Alert in Canada, Ny-Ålesund in Svalbard,  
Barrow in Alaska, Pallastunturi in Finland, and Fukue in Japan, and stable for up to 10 years. We  
successfully estimated  $\text{MAC}_{\text{cor}}$  values (10.6–15.2  $\text{m}^2 \text{g}^{-1}$  at a wavelength of 550 nm) for these  
instruments and these  $\text{MAC}_{\text{cor}}$  values can be used to obtain error-constrained estimates of  $M_{\text{BC}}$  from  $b_{\text{abs}}$   
measured at these sites even in the past, when COSMOS measurements were not made. Because the  
60 absolute values of  $M_{\text{BC}}$  in these Arctic sites estimated by this method are consistent with each other,  
they are applicable to the study of spatial and temporal variation of  $M_{\text{BC}}$  in the Arctic and to evaluation  
of the performance of numerical model calculations.



## 65 1 Introduction

Black carbon (BC) aerosols strongly absorb solar radiation and thereby impact the radiation budget in the Arctic (Bond et al., 2013; AMAP, 2015). In addition, BC deposited on snow decreases the snow surface albedo and accelerates snowmelt (AMAP, 2015; Flanner et al., 2009). According to recent  
70 Eyring et al., 2016), BC contributes the second largest positive radiative forcing in the Arctic, after carbon dioxide (CO<sub>2</sub>) (Oshima et al., 2020). BC is one of the short-lived climate forcers (SLCF) and reductions of BC emissions can decrease the positive Arctic radiative forcing over much shorter timescales than can reductions of CO<sub>2</sub> emissions (Sand et al., 2016). Long-term measurements of mass concentrations of BC in the atmosphere ( $M_{BC}$  [ $\mu\text{g m}^{-3}$ ]) at various locations provide fundamental data  
75 for the detection of long-term trends in  $M_{BC}$  in the Arctic that are associated with changes in BC emissions. Such  $M_{BC}$  data are also useful for validation and improvement of climate models. However, because many long-term surface instruments measure aerosol light absorption coefficient ( $b_{abs}$  [ $\text{Mm}^{-1}$ ]) rather than  $M_{BC}$ , there are large uncertainties in  $M_{BC}$  estimated from the measurements of  $b_{abs}$ ; these uncertainties have not been critically evaluated.

80 A continuous soot monitoring system called COSMOS (Kanomax, Osaka, Japan) has been developed to measure  $M_{BC}$  (Miyazaki et al., 2008; Kondo et al., 2009, 2011). This filter-based absorption photometer is equipped with an inlet that is heated to 300°C to remove non-refractory components from the aerosol phase. COSMOS  $M_{BC}$  values ( $M_{BC}$  (COSMOS)) have been compared with those measured by a single particle soot photometer (SP2; Droplet Measurement Technologies, Longmont, CO, USA;  $M_{BC}$  (SP2)),  
85 which is based on a laser-induced incandescence technique (Schwarz et al., 2006; Moteki and Kondo, 2010); simultaneous measurements in Asia and at Ny-Ålesund in Svalbard have shown that  $M_{BC}$  (SP2) and  $M_{BC}$  (COSMOS) agree to within about 10 % (Kondo et al., 2009, 2011; Ohata et al., 2019).

Long-term measurements of  $b_{abs}$  at various sites have been carried out by other types of filter-based absorption photometers, including the particle absorption soot photometer (PSAP; Radiance Research,  
90 Seattle, WA, USA), the continuous light absorption photometer (CLAP; NOAA, Boulder, CO, USA; Ogren et al., 2017), the Aethalometer (Magee Scientific, Berkeley, CA, USA), and the multi-angle absorption photometer (MAAP; Thermo Scientific, Waltham, MA, USA) (e.g., Schmeisser et al., 2018). Measurements of light-absorption and light-scattering properties of aerosols are important for constraining their interannual and seasonal variability, potential particle sources, and resulting aerosol-  
95 radiation interactions in the Earth system (Schmeisser et al., 2018; Bellouin et al., 2020). However, the accuracy and stability of conversion of  $b_{abs}$  obtained by these instruments to  $M_{BC}$  have not yet been fully evaluated, mainly because of a lack of simultaneous and reliable long-term  $M_{BC}$  measurements. The



relationship between  $b_{\text{abs}}$  obtained by these instruments and  $M_{\text{BC}}$  are complicated by complex contributions from mixing states of BC (i.e., lensing effect by BC-coating materials; Bond et al., 2006; Lack et al., 2008), other co-existing light-absorbing aerosols such as brown carbon and mineral dust, and measurement artifacts by light-scattering aerosols on filters (Bond et al., 1999). Evaluations that have been completed to date include those of Kanaya et al. (2013, 2020), who compared  $M_{\text{BC}}$  (COSMOS) with the  $b_{\text{abs}}$  measured by MAAP ( $b_{\text{abs}}$  (MAAP)) on Fukue Island, Japan, and Sinha et al. (2017), who compared  $b_{\text{abs}}$  measured by PSAP ( $b_{\text{abs}}$  (PSAP)) at Barrow in Alaska and Ny-Ålesund (Zeppelin station), Svalbard. The results of these studies showed that  $b_{\text{abs}}$  (MAAP) and  $b_{\text{abs}}$  (PSAP) were strongly correlated with  $M_{\text{BC}}$  (COSMOS), making it possible to convert  $b_{\text{abs}}$  to  $M_{\text{BC}}$  at these sites with reasonable accuracy. Long-term observations of  $b_{\text{abs}}$  have been made also at Arctic sites Alert in Canada by PSAP and Aethalometer (Sharma et al., 2004, 2006, 2017), Ny-Ålesund by Aethalometer (Eleftheriadis et al., 2009), and Pallastunturi in Finland by MAAP (Hyvärinen et al., 2011; Lihavainen et al., 2015). To investigate the possibility of converting  $b_{\text{abs}}$  to  $M_{\text{BC}}$  at each of these sites, it is important to simultaneously measure  $M_{\text{BC}}$  and  $b_{\text{abs}}$  by collocating a COSMOS (or SP2) at each site with each of these filter-based absorption photometer instruments.

The conversion of  $b_{\text{abs}}$  obtained by these instruments to  $M_{\text{BC}}$  can be made by assuming a reasonable conversion factor, i.e., the value of mass absorption cross section (MAC [ $\text{m}^2 \text{g}^{-1}$ ];  $M_{\text{BC}} = b_{\text{abs}}/\text{MAC}$ ). The MAC values can depend on location because the spatiotemporal variations in microphysical properties of BC (i.e., mixing states and size distributions) and properties of co-existing light-absorbing and scattering aerosols will affect  $b_{\text{abs}}$  measurements. The plausible MAC values for conversion can also depend on the type of instrument because each instrument uses different wavelength and adopts various correction methods for quantifying  $b_{\text{abs}}$ . Despite several intercomparisons and field experiments (Asmi et al., 2020) as well as thorough assessment of these techniques (Lack et al., 2008; Moosmüller et al., 2009) the simultaneous changes in aerosol source region, mixing state, concentration and particle optical size are reflected in the instruments' response in a complex way and with a variable level of uncertainty.

In general, the MAC of BC, here simply denoted as “ $\text{MAC}_{\text{BC}}$ ” for both bare and internally-mixed BC, is a fundamental optical parameter that relates  $M_{\text{BC}}$  with  $b_{\text{abs}}$  of BC ( $b_{\text{abs,BC}}$ ) in climate models (i.e.,  $b_{\text{abs,BC}} = M_{\text{BC}} \times \text{MAC}_{\text{BC}}$ ). Bond and Bergstrom (2006) reported the  $\text{MAC}_{\text{BC}}$  value of  $7.5 \text{ m}^2 \text{g}^{-1}$  at a wavelength of 550 nm for combusted fresh BC. Cho et al., (2021) estimated  $\text{MAC}_{\text{BC}}$  values of 6–12  $\text{m}^2 \text{g}^{-1}$  at 550 nm in the Asian outflow using aircraft-based SP2 data and Mie theory. Yuan et al. (2021) showed that the  $\text{MAC}_{\text{BC}}$  values at 870 nm at a rural site in Germany clearly increased as the coating thickness of BC increased.

However, in this paper we focus on the MAC values mainly from the viewpoint of a conversion factor to obtain error-constrained  $M_{\text{BC}}$  from the  $b_{\text{abs}}$  measurements by the filter-based absorption photometers





because such  $M_{BC}$  data will be the observational base for understanding long-term trends and spatial distributions of BC in the Arctic. Detailed investigations of the accuracy of the absolute values of  $b_{abs}$  measured at each site are beyond the scope of this study.

We critically re-examine the concepts underpinning the use of filter-based instruments to estimate  $M_{BC}$ . We derive MAC values for PSAP/CLAP, Aethalometer, and MAAP measurements based on their comparison with COSMOS measurements at the four above-mentioned Arctic sites (Alert, Ny-Ålesund, Barrow, and Pallastunturi) and one East Asian site (Fukue). The variability of the derived MAC values and their dependencies on observation site and instrument type are analyzed. We also compare  $M_{BC}$  values measured by COSMOS and SP2 at Alert and Fukue to confirm their agreement under different environmental conditions.

## 2 Methods

### 2.1 Observation sites

Measurements of  $b_{abs}$  by the various types of filter-based absorption photometers were compared with measurements of  $M_{BC}$  by COSMOS at Arctic sites Alert in Canada (82.5° N, 62.5° W; Sharma et al., 2017), Ny-Ålesund (Zeppelin station) in Svalbard (78.9° N, 11.9° E; Sinha et al., 2017), Barrow in Alaska (71.3° N, 156.6° W; Sinha et al., 2017), and Pallastunturi (Pallas, hereafter) in Finland (68.0° N, 24.0° E; Hyvärinen et al., 2011), as summarized in Table 1 and Fig. 1. Along with these sites, comparisons were also made at a remote site on Fukue Island (32.8° N, 128.7° E; Kanaya et al., 2020) in Japan, where air masses from the Asian continent are occasionally transported to the site and properties of aerosols should be distinctly different from those at the Arctic sites. Instruments used at each site are listed in Table 1 and described in the following section.

### 2.2 Instruments

#### 2.2.1 SP2

In this study we used the SP2 and COSMOS as standard instruments to measure  $M_{BC}$ . Detailed descriptions of the SP2, including calibration methods, are given elsewhere (Schwarz et al., 2006; Moteki and Kondo, 2010). Briefly, the SP2 uses the laser-induced incandescence technique and detects BC on a single-particle basis. We used two SP2s in this study: the one installed at Fukue was maintained and calibrated by the University of Tokyo (UT-SP2, hereafter) and the other one at Alert was maintained and calibrated by Environmental and Climate Change Canada (EC-SP2, hereafter). The configuration of the UT-SP2 is identical to that described by Moteki and Kondo (2010). The model designation of the EC-SP2 was “SP2-D” with eight channels. The UT-SP2 and EC-SP2 measured BC size distributions in the mass-equivalent diameter ( $D_m$ ) range 70–850 and 60–600 nm, respectively. The void-free density of BC was assumed to be 1.8 g cm<sup>-3</sup>. These SP2s were calibrated using fullerene soot



particles (Alfa Aeser, stock #40971, lot #FS12S011; Moteki and Kondo, 2010; Kondo et al., 2011). The laser-induced incandescence signal intensity of the UT-SP2 for the specific mass of ambient BC particles in Tokyo agree with that of fullerene soot particles to within about 10 % (Kondo et al., 2011). Laborde et al. (2012) reported similar SP2 calibration curves for fullerene soot particles, diesel exhaust, and ambient BC particles in Switzerland. The accuracy of  $M_{BC}$  (SP2) estimated from the uncertainty of the calibration and operational conditions of SP2 was about 10 %. No particle-size cut was used for the inlet of the UT-SP2, whereas a  $PM_{10}$  cyclone was used for the EC-SP2.

## 2.2.2 COSMOS

### 2.2.2.1 Measurements of $M_{BC}$ by COSMOS

The principles of operation of the COSMOS apparatus are detailed in previous papers (Miyazaki et al., 2008; Kondo et al., 2011; Kondo, 2015; Ohata et al., 2019). Briefly, the COSMOS measures the extinction coefficient ( $b_0$ ) of aerosols collected on a quartz-fiber filter at a given wavelength ( $\lambda = 565$  nm). Most previous studies used filters from Pallflex (E70-2075W, Pall, Port Washington, NY, USA), which are no longer available. Consequently, HEPA filters have been used for more recent observations (Irwin et al., 2015), including this study. An important difference between the COSMOS and the other types of filter-based absorption photometer is that the inlet of the COSMOS is heated to 300°C to remove volatile light scattering particles (LSPs) and coatings of BC from the aerosol phase. Therefore, the effect on  $b_0$  of co-existing volatile components externally or internally mixed with BC particles can be ignored. The COSMOS is equipped with a  $PM_{10}$  cyclone to minimize the effect in coarse mode of refractory non-BC particles, such as dust and sea-salt particles. Consequently, the absorption coefficient for the COSMOS is given as

$$b_{\text{abs}}(\text{COSMOS}) = f_{\text{fil}} b_0. \quad (1)$$

Here,  $f_{\text{fil}}$  is a factor used to correct for the increase of absorption caused by multiple scattering in the filter medium (Bond et al., 1999; Ogren, 2010; Ohata et al., 2019). The MAC for the COSMOS [ $\text{m}^2 \text{g}^{-1}$ ] is operationally defined as

$$\text{MAC}(\text{COSMOS}, \text{SP2}) \equiv \frac{b_{\text{abs}}(\text{COSMOS})}{M_{BC}(\text{SP2})}, \quad (2)$$

where the numerator and denominator, respectively, are simultaneous measurements of  $b_{\text{abs}}$  [ $\text{Mm}^{-1}$ ] by COSMOS and  $M_{BC}$  [ $\mu\text{g m}^{-3}$ ] by SP2 for ambient air. The MAC value for a Pallflex filter at  $\lambda = 565$  nm was previously set at 8.73 [ $\text{m}^2 \text{g}^{-1}$ ] (Sinha et al., 2017). For a HEPA filter, the MAC is about 6 % higher (Irwin et al., 2015). Depending on the filters used (Pallflex or HEPA), the appropriate MAC value was used in this study.

Once the MAC (COSMOS, SP2) is determined,  $M_{BC}$  (COSMOS) [ $\text{g m}^{-3}$ ] at standard temperature and pressure (0°C, 1013 hPa) can be estimated as



$$M_{\text{BC}}(\text{COSMOS}) = \frac{b_{\text{abs}}(\text{COSMOS})}{\text{MAC}(\text{COSMOS}, \text{SP2})}. \quad (3)$$

200 One particular purpose of the heating of sampled air to 300°C is to make the MAC (COSMOS, SP2) stable and independent of original mixing states of BC particles. In other words, the heating treatment makes  $b_{\text{abs}}(\text{COSMOS})$  more proportional to BC mass concentrations, as compared to the other filter-based absorption photometers described in Sect. 2.2.3. As a consequence, unlike the other filter-based absorption photometers, the absorption coefficient of unheated original aerosols is not provided by  
205 COSMOS. Thus, the COSMOS has been developed to measure  $M_{\text{BC}}$ , not  $b_{\text{abs}}$ . In this sense,  $M_{\text{BC}}(\text{COSMOS})$  is different from “equivalent” BC mass concentrations estimated from the unheated  $b_{\text{abs}}$  measurements (Petzold et al., 2013).

We call the COSMOS that was calibrated by comparison with the SP2 in Tokyo the “standard COSMOS”, described hereafter as Std-COSMOS. Because the MAC of the Std-COSMOS was  
210 determined by comparison with SP2 (Eq. (2)), it acts as a transfer standard for the SP2. The  $b_{\text{abs}}(\text{COSMOS})$  of each COSMOS manufactured is compared with the Std-COSMOS by sampling ambient BC particles in Osaka, Japan, typically for 1–2 weeks. The comparisons during these periods were statistically reliable partly due to relatively high BC concentrations in Osaka. The  $b_{\text{abs}}(\text{COSMOS})$  of 28  
215 COSMOS instruments manufactured thus far agree with that of Std-COSMOS to within about  $\pm 7\%$ , indicating reliable quality control in manufacturing. The small differences originating from the uncertainty of the filter sampling spot size of each unit are corrected for in deriving  $M_{\text{BC}}(\text{COSMOS})$ .

It is important to compare  $M_{\text{BC}}(\text{COSMOS})$  and  $M_{\text{BC}}(\text{SP2})$  outside Tokyo and Osaka, to confirm both the strong correlation between  $M_{\text{BC}}(\text{COSMOS})$  and  $M_{\text{BC}}(\text{SP2})$  and the long-term stability of the MAC (COSMOS) value. Ohata et al. (2019) made these comparisons at two remote sites: at Cape Hedo  
220 (26.9°N, 128.3°E), Japan, and at Ny-Ålesund. At each of these locations, the concentrations of BC and LSP and the mixing states of BC were considerably different from those in Tokyo and Osaka.  $M_{\text{BC}}(\text{COSMOS})$  and  $M_{\text{BC}}(\text{SP2})$  agree to within about 10 % at these sites, thus demonstrating the validity of using the Std-COSMOS to calibrate each of the COSMOS instruments to be used for field observations. Ohata et al. (2019) also showed that the dependencies of MAC (COSMOS) on the thickness of coatings  
225 of BC particles,  $M_{\text{BC}}$ , and volume concentrations of the co-existing LSPs were small. Although the MAC (COSMOS) showed a slight dependence on the mass size distributions of BC, the sensitivity of the MAC (COSMOS) to such variations in microphysical properties of BC was generally less than 10 % (Kondo et al., 2011; Ohata et al., 2019).

Previously estimated uncertainties of  $M_{\text{BC}}(\text{COSMOS})$  were about 10 % based on the range of  
230 agreement between  $M_{\text{BC}}$  measurements by COSMOS and UT-SP2 (Kondo et al., 2011; Ohata et al., 2019). It may be more appropriate to estimate the absolute accuracy of  $M_{\text{BC}}(\text{COSMOS})$  to be about 15 %, including the above-mentioned 10 % uncertainty of  $M_{\text{BC}}(\text{SP2})$ . This 15 % uncertainty also covers



the range of agreement between  $M_{BC}$  (COSMOS) and  $M_{BC}$  (SP2) previously reported by other groups at Ny-Ålesund (Zannata et al., 2018) and at Fukue (Miyakawa et al., 2017).

235 Although we used the SP2 and COSMOS as standard instruments to measure  $M_{BC}$  in this study, thermal-optical analysis, which quantifies elemental carbon (EC) mass concentrations ( $M_{EC}$ ), also has been a traditional standard method to measure BC. Measurements of  $M_{EC}$  can depend on the temperature protocol and optical charring correction method used (e.g., Bond et al., 2013). Agreements within 10 % of  $M_{BC}$  (SP2),  $M_{BC}$  (COSMOS), and  $M_{EC}$  were reported by Kondo et al. (2011), whereas

240 systematic differences between  $M_{BC}$  (SP2) and  $M_{EC}$  up to a factor of 2 were found by Pileci et al. (2021). Although the difference between  $M_{BC}$  (COSMOS) and  $M_{EC}$  was generally lower than  $5 \text{ ng m}^{-3}$  at the Arctic site Barrow (Sinha et al., 2017), this difference can be important for pristine summer Arctic conditions ( $M_{BC}$  (COSMOS)  $< 20 \text{ ng m}^{-3}$ ). Considering these previously reported agreements and discrepancies between  $M_{BC}$  (SP2 or COSMOS) and  $M_{EC}$ , in some cases the MAC values determined by

245  $b_{\text{abs}}$  and  $M_{BC}$  measurements (this study) can differ from those determined by  $b_{\text{abs}}$  and  $M_{EC}$  measurements (Zanatta et al., 2016).

#### 2.2.2.2 Effect of light-absorbing $\text{FeO}_x$ particles on $M_{BC}$ (COSMOS)

Light-absorbing iron oxide ( $\text{FeO}_x$ ) aerosols, which the SP2 can distinguish from BC (Yoshida et al., 2016; Lamb, 2019), can affect  $M_{BC}$  measured by filter-based absorption photometers.  $\text{FeO}_x$  aerosols are

250 emitted from both anthropogenic sources (e.g., motor vehicle exhaust) and natural sources (e.g., wind-blown mineral dust). Within the detectable diameter range of the UT-SP2 ( $D_m = 70\text{--}850 \text{ nm}$  for BC and  $D_m = 170\text{--}2100 \text{ nm}$  for  $\text{FeO}_x$ ), the mass concentration ratios of  $\text{FeO}_x$  to BC were typically  $\sim 0.4$  in East Asia and  $\sim 0.2$  in the Arctic; they were mainly of anthropogenic origin in both regions (Moteki et al., 2017; Ohata et al., 2018; Yoshida et al., 2018, 2020).  $\text{FeO}_x$  aerosols contribute at least 4–7 % of the

255 short-wave absorbing powers of BC in Asian continental outflows (Moteki et al., 2017) and their direct radiative forcing has been estimated to be  $0.22 \text{ W m}^{-2}$  over East Asia (Matsui et al., 2018). Here, we estimate the effect of light absorption by  $\text{FeO}_x$  on  $M_{BC}$  measured by the COSMOS. The ratio of light absorbed by  $\text{FeO}_x$  to that absorbed by BC at a wavelength  $\lambda$  ( $\varepsilon(\lambda)$ ) is given by

$$\varepsilon(\lambda) = \frac{\int_{D_L}^{D_U} \frac{dM_{\text{FeO}_x}}{d \log D_m} \text{MAC}_{\text{Mie\_FeO}_x}(D_m, \lambda) d \log D_m}{\int_{D_L}^{D_U} \frac{dM_{\text{BC}}}{d \log D_m} \text{MAC}_{\text{Mie\_BC}}(D_m, \lambda) d \log D_m}, \quad (4)$$

260 where  $D_m$  is mass equivalent diameter of bare BC or  $\text{FeO}_x$ ;  $D_L$  and  $D_U$  are the lower and upper limits, respectively, of the diameter for the integral calculus;  $dM_{\text{BC}}/d \log D_m$  and  $dM_{\text{FeO}_x}/d \log D_m$  are the mass size distributions of BC and  $\text{FeO}_x$ , respectively; and  $\text{MAC}_{\text{Mie\_BC}}(D_m, \lambda)$  and  $\text{MAC}_{\text{Mie\_FeO}_x}(D_m, \lambda)$  are the MAC values of bare BC and  $\text{FeO}_x$ , respectively, for  $D_m$  and  $\lambda$  calculated by Mie theory.

The mass size distributions of BC and  $\text{FeO}_x$  at Fukue and Ny-Ålesund (Fig. 2) were obtained by fitting

265 monomodal and bimodal lognormal functions to the average mass size distributions measured by the



SP2 during each observation campaign (Yoshida et al., 2020). The measurements at Fukue were made in April 2019 and those at Ny-Ålesund in March 2017. The  $MAC_{Mie\_BC}(D_m, \lambda)$  and  $MAC_{Mie\_FeO_x}(D_m, \lambda)$  data (Fig. 2) were calculated by Mie theory for  $\lambda = 565$  nm (wavelength used for COSMOS). For this calculation, we assumed BC and  $FeO_x$  to be in the form of bare spheres with void-free densities of 1.80 g cm<sup>-3</sup> and 5.17 g cm<sup>-3</sup>, respectively. The refractive index of BC we used was  $1.99 + 0.64i$ , which is the value for BC at  $\lambda = 600$  nm (Bergstrom, 1972). The refractive index of  $FeO_x$  we used was  $2.56 + 0.57i$ , which is the value for magnetite at  $\lambda = 600$  nm (Huffman and Stapp, 1973).

From Eq. (4), the  $\varepsilon$  values at Fukue and Ny-Ålesund were calculated to be 3.6 % and 1.9 %, respectively, for  $(D_L, D_U) = (30, 1000)$  nm. These  $\varepsilon$  values became 4.6 % and 2.6 % for  $(D_L, D_U) = (30, 2500)$  nm). Because COSMOS is equipped with a  $PM_{10}$  cyclone, we estimated the effect of light absorption by  $FeO_x$  on  $M_{BC}$  measured by COSMOS to be < 4 % in East Asia and < 2 % in the Arctic. Note that these estimates are upper limits of the effect of  $FeO_x$  because the  $PM_{10}$  cyclone is designed to remove particles of > 1  $\mu$ m aerodynamic diameter ( $D_a$ ). Due to the fractal shape and high density of  $FeO_x$  particles (Moteki et al., 2017),  $D_m$  is considerably smaller than  $D_a$  for  $FeO_x$  particles and thus  $D_U$  in Eq. (4) should be less than 1  $\mu$ m.

The effect of  $FeO_x$  on  $M_{BC}$  (COSMOS) should be even smaller considering that the mass concentration of anthropogenic  $FeO_x$  is correlated with  $M_{BC}$ , as mentioned above. Even if  $b_{abs}$  (COSMOS) is enhanced by  $FeO_x$  by a few percent, this effect is already incorporated to some extent, by operationally defining MAC (COSMOS, SP2) by Eq. (2).

The effect of  $FeO_x$  on  $b_{abs}$  may be somewhat higher for the other filter-based absorption photometers than for COSMOS if they are equipped with a larger particle size cut ( $PM_{2.5}$  or  $PM_{10}$ ). For accurate measurements of  $M_{BC}$ , the use of a  $PM_{10}$  cyclone or impactor is recommended to minimize the effects of  $FeO_x$ , as well as other refractory particles such as natural dust and sea-salt particles.

## 2.2.3 Filter-based absorption photometers other than COSMOS

### 2.2.3.1 PSAP and CLAP

The principle of operation of the PSAP is similar to those of COSMOS (Bond et al., 1999; Sinha et al., 2017). In this study, we also used  $b_{abs}$  data obtained with a continuous light absorption photometer (CLAP) (Ogren et al., 2017). The CLAP is conceptually similar to the PSAP but uses solenoid valves to cycle through eight sample filter spots. The PSAP and CLAP both utilize the Pallflex filters. The unit-to-unit variations of the PSAP and CLAP were reported to be within 6 % (Bond et al., 1999) and 4 % (Ogren et al., 2017), respectively. The wavelengths of the light absorption measured by either PSAP or CLAP at Barrow, Ny-Ålesund, and Alert were about 467, 530, and 660 nm. The major difference of the PSAP and CLAP from the COSMOS is that the sample air inlets of the PSAP and CLAP are not heated



to 300°C. Therefore, the effect of the attenuation of light by LSPs is corrected for by using the aerosol  
300 light scattering coefficient simultaneously measured by an integrating nephelometer (Bond et al., 1999;  
Ogren 2010). This correction adjusts for measurement artifacts but introduces uncertainties in the  
estimate of  $b_{\text{abs}}$  (PSAP or CLAP). At the above three sites, light scattering coefficients measured by  
nephelometers at wavelengths of 450, 550, and 700 nm were used for this correction. The  $b_{\text{abs}}$  for the  
PSAP or CLAP (hereafter,  $b_{\text{abs}}$  (PSAP/CLAP)) at  $\lambda = 550$  nm was obtained by adjusting measured  
305 absorption at 530 to 550 nm by using the  $\lambda^{-1}$  relationship (Sinha et al., 2017; Sharma et al., 2017).  
Schmeisser et al. (2017) reported that the median value of the absorption Ångström exponent at Arctic  
sites was 1.04, which supports our assumption of the  $\lambda^{-1}$  relationship. The accuracy of the  $b_{\text{abs}}$  measured  
by PSAP ranges between 20 and 30% (Bond et al., 2013).

### 2.2.3.2 Aethalometer

310 An AE-31 Aethalometer (Hansen et al., 1984) has been used for measurements of  $b_{\text{abs}}$  at Alert without  
any particle size cut (Sharma et al., 2017). This Aethalometer measures the attenuation (ATN) of light  
transmitted through particles accumulating on a quartz fiber filter at seven wavelengths (370, 470, 520,  
590, 660, 880, and 950 nm). In deriving  $b_{\text{abs}}$  (Aethalometer) from ATN data, the correction factor  $C_f =$   
3.45 (Backman et al., 2017) was applied. This correction factor is very close to the correction factor  $C_0$   
315  $= 3.5$  recommended by the World Meteorological Organization/Global Atmosphere Watch (2016).

Another AE-31 Aethalometer has also been used at Ny-Ålesund (Zeppelin station) (Eleftheriadis et al.,  
2009), where the sampling inlet was equipped with a calculated PM<sub>10</sub> size cut. Data post-processing  
included flagging based on Zeppelin station logs, Ny-Ålesund harbor logs and diagnostics reported by  
the instrument (flowrate, raw attenuation, zero signal, etc). A correction factor  $C_0 = 3.5$  was used to  
320 compensate for the multiple scattering effect.

The filter loading effect is not significant for Arctic aerosol, as reported by Backman et al. (2017). For  
Alert, the slope of the correction factor  $C_f - 1$  to ATN is  $k = 0.00074$ , indicating a 5 % difference at an  
ATN value of 80. For Zeppelin, the loading effect causes a 2 % difference in  $C_f$  at an attenuation value  
of 80. These uncertainties are considered small compared to the overall  $b_{\text{abs}}$  uncertainty, which is 20–  
325 30 % (Bond et al., 2013). Therefore, the loading correction is not applied to the AE31 measurements.  
Corrections for light scattering by using nephelometer data were also not applied.

### 2.2.3.3 MAAP

Detailed descriptions of the MAAP are given elsewhere (Petzold et al., 2002, 2005; Petzold and  
Schönlinner, 2004; Kanaya et al., 2013). In brief, the MAAP monitors the transmittance of light through a  
330 glass-fiber tape and measures reflectance at two angles. To remove the influence of LSPs,  $b_{\text{abs}}$  (MAAP)  
from particles deposited on the filter is derived by radiative transfer calculations. The uncertainty of  $b_{\text{abs}}$   
(MAAP) was estimated by Petzold and Schönlinner (2004) to be 12%. The unit-to-unit variation of the



MAAP was reported to be within 5% (Müller et al., 2011). The MAC values for the MAAP (MAC (MAAP)) for  $\lambda = 637$  nm was determined by comparing  $b_{\text{abs}}$  (MAAP) and  $M_{\text{BC}}$  measured at four sites in  
335 Germany by the German reference method VDI2465 Part 1 (GRM; Schmid et al., 2001), represented by

$$\text{MAC (MAAP, GRM)} \equiv \frac{b_{\text{abs}}(\text{MAAP})}{M_{\text{BC}}(\text{GRM})}. \quad (5)$$

For the measurements of  $M_{\text{BC}}$  (GRM), organic carbon was removed by solvent extraction and the residual BC particles on the filters were oxidized to  $\text{CO}_2$  and quantified by coulometric titration. The measurement uncertainty of  $M_{\text{BC}}$  (GRM) was about 25 % (Petzold and Schönlinner, 2004). The MAC of  $6.6 \text{ m}^2 \text{ g}^{-1}$  is the  
340 default setting by the manufacturer based on their study. In determining MAC (MAAP, GRM), an SP2 was not used to measure  $M_{\text{BC}}$ , and this is a potential source of discrepancy in this value of MAC, as discussed in Sect. 3.4.1 and 3.5.2.

### 3 Results and discussion

#### 3.1 Alert

##### 345 3.1.1 COSMOS-SP2 comparison

Long-term measurements of BC using different manufacturer's model versions of SP2s have been conducted at Alert since 2011 (Sharma et al., 2017). In this study, we used the data obtained by an EC-SP2 (model "SP2-D" with eight channels; see Sect. 2.2.1) from January to May 2018 for comparison with the COSMOS data. The EC-SP2 and COSMOS aspirated sample air from a common inlet with a  
350  $\text{PM}_{10}$  size cut. Fig. 3a shows the number and mass size distributions of BC averaged over the observation period. The mode diameter of the average mass size distribution of BC was  $\sim 210$  nm, which is similar to that previously reported at Alert (Sharma et al., 2017) and that observed by aircraft-based measurements over Alert (Schulz et al., 2019). Because the upper limit of the detectable diameter range of BC was  $\sim 600$  nm for the EC-SP2, we have estimated  $M_{\text{BC}}$  (SP2) over the range up to 1000 nm  
355 by fitting lognormal functions to the measured mass size distributions. The time series of hourly values of  $M_{\text{BC}}$  (COSMOS) and  $M_{\text{BC}}$  (SP2) (Fig. 3b) were strongly correlated ( $r^2 = 0.92$ ;  $r^2$  is the square of the correlation coefficient) and the slope of the regression forced through the origin was 1.02 (Fig. 3c). These results show that on average, the agreement between  $M_{\text{BC}}$  (COSMOS) and  $M_{\text{BC}}$  (SP2) at Alert was within 10 %.

360 Although this agreement was consistent with those reported in previous studies using UT-SP2 (Kondo et al., 2011; Ohata et. al., 2019), note that there were some differences between  $M_{\text{BC}}$  (SP2) measured by the EC-SP2 and that by the UT-SP2. The EC-SP2 was calibrated by Aquadag samples at Alert during the observation period and also calibrated by fullerene soot samples at the Paul Scherrer Institute in Switzerland after the observation period. Because the sensitivity of the incandescence signals of the SP2  
365 to Aquadag is higher than that to fullerene soot, the calibration curve for Aquadag needs correction to





obtain the fullerene-soot equivalent calibration curve (Baumgardner et al., 2012). Additionally, to make this correction, assumptions of the effective density ( $\rho_{\text{eff}}$ ) values of Aquadag (Moteki and Kondo, 2010; Gysel et al., 2011), which depend on the mobility diameter of Aquadag, are needed since a differential mobility analyzer (DMA) is used for the on-site calibration at Alert instead of an aerosol particle mass analyzer (APM) or a centrifugal particle mass analyzer. The  $\rho_{\text{eff}}$  values of Aquadag samples can depend on their batches (Gysel et al., 2011). In the previous study by Sharma et al. (2017), the constant value of  $\rho_{\text{eff}}$  ( $= 0.7 \text{ g cm}^{-3}$ ) for Aquadag was assumed to derive  $M_{\text{BC}}$  (SP2) at Alert. However, we have found that  $M_{\text{BC}}$  (SP2) at Alert highly depended on the assumed  $\rho_{\text{eff}}$  values of Aquadag used for the on-site calibration with a DMA. Because of this, we used the calibration curve obtained by fullerene soot with an APM at the Paul Scherrer Institute after the observation period for this study. The conditions of the EC-SP2 might have differed slightly between during and after the observation period, which may lead to additional uncertainties for  $M_{\text{BC}}$  (SP2) at Alert, although the difference of Aquadag calibrations made before and after the campaign was less than about 10 %. In addition, the upper limit of the detectable diameter of BC for the EC-SP2 ( $D_m \sim 600 \text{ nm}$ ) was lower than that for the UT-SP2 ( $D_m \sim 850 \text{ nm}$ ), although the above-mentioned extrapolation up to 1000 nm was made to derive  $M_{\text{BC}}$  (SP2) at Alert. Despite these differences between EC-SP2 and UT-SP2,  $M_{\text{BC}}$  (COSMOS) and  $M_{\text{BC}}$  (SP2) agree to within 10 % at Alert, consistent with previous studies that reported the stability of the relationship between  $M_{\text{BC}}$  (COSMOS) and  $M_{\text{BC}}$  (SP2) at various sites (Kondo et al., 2011; Ohata et al., 2019).

### 3.1.2 COSMOS-PSAP comparison

Measurements of  $M_{\text{BC}}$  (COSMOS) at Alert began in January 2018. A  $\text{PM}_{10}$  cyclone was used for the COSMOS and a  $\text{PM}_{10}$  impactor for the PSAP and two CLAP instruments (CLAP1, CLAP2). The time series of 1-h and 24-h averaged  $M_{\text{BC}}$  (COSMOS) were strongly correlated with  $b_{\text{abs}}$  (PSAP;  $\lambda = 550 \text{ nm}$ ) for 2018–2019 ( $r^2 \sim 0.96$ ; Fig. 4a–d). In this study, we define the MAC value,  $\text{MAC}_{\text{cor}}$ , as the slope of the least squares regression forced through the origin in the correlation plot. The values of  $\text{MAC}_{\text{cor}}$  (PSAP;  $\lambda = 550 \text{ nm}$ ) for the whole period were  $13.9 \text{ m}^2 \text{ g}^{-1}$  and  $14.0 \text{ m}^2 \text{ g}^{-1}$  for the 1-h and 24-h averaged data, respectively, as summarized in Table 2. The results of the same analyses for other wavelengths of the PSAP and the two CLAPs show that the strength of the correlation depended little on wavelength (Table 2). The  $b_{\text{abs}}$ , and therefore the MAC, for the PSAP and the two CLAP instruments (CLAP1, CLAP2) agree to within 8%, indicating little difference in the performance of these instruments.

Along with the correlation analysis, variability of the  $b_{\text{abs}}$  (PSAP) /  $M_{\text{BC}}$  (COSMOS) ratio was also analyzed for the 1-h and 24-h data (Fig. 4e and f). This ratio can be interpreted as an hourly or daily MAC value at each time. Because this ratio tends to be unstable when the  $M_{\text{BC}}$  (COSMOS) values are very low, we set a threshold  $M_{\text{BC}}$  (COSMOS) value of  $2 \text{ ng m}^{-3}$  in this analysis, as shown in these figures. The median ratio, defined as median MAC and denoted as  $\text{MAC}_{\text{med}}$ , was  $13.5 \text{ m}^2 \text{ g}^{-1}$  for both 1-



h and 24-h data, which is very close to  $MAC_{cor}$  ( $13.9 \text{ m}^2 \text{ g}^{-1}$  and  $14.0 \text{ m}^2 \text{ g}^{-1}$  for the 1-h and 24-h data, respectively) (Table 3). The difference between  $MAC_{cor}$  and  $MAC_{med}$  was about 4 %, leading to the same difference between the estimated  $M_{BC}$  values if these MAC values are used for conversion of  $b_{abs}$  (PSAP) to  $M_{BC}$ . Based on the interquartile ranges of the  $b_{abs}$  (PSAP) /  $M_{BC}$  (COSMOS) ratios (Fig. 4e and f), variations of the ratios (with an  $M_{BC}$  threshold of  $2 \text{ ng m}^{-3}$ ), denoted as  $V_{MAC}$ , were within 19 % and 18 % of the  $MAC_{med}$  values for the 1-h and 24-h data, respectively (Table 3). Therefore, conversion of 1-h and 24-h averaged  $b_{abs}$  (PSAP;  $\lambda = 550 \text{ nm}$ ) data to  $M_{BC}$  by assuming a constant  $MAC_{med}$  leads to uncertainty of about 19 % at Alert. We used the same method in estimating  $MAC_{cor}$ ,  $MAC_{med}$ , and  $V_{MAC}$  for other instruments and other locations, as summarized in Table 3. Note that this estimated uncertainty can depend on the threshold value of  $M_{BC}$  (COSMOS) assumed in the analysis. The relative uncertainty becomes higher (lower) in summer (winter/spring) when the  $M_{BC}$  values tend to be low (high) (Fig. 4a and b).

### 3.1.3 COSMOS–Aethalometer comparison

Measurements of  $b_{abs}$  at Alert were made by an Aethalometer at wavelengths of 370, 470, 520, 590, 660, 880, and 950 nm without any particle size cut. Time series of  $b_{abs}$  (Aethalometer;  $\lambda = 590 \text{ nm}$ ) and  $M_{BC}$  (COSMOS) in 2018–2019 are shown in Fig. S1 in the Supplement.  $b_{abs}$  (Aethalometer;  $\lambda = 590 \text{ nm}$ ) was highly correlated ( $r^2 > 0.90$ ) with  $M_{BC}$  (COSMOS) (Fig 5a and b). The  $MAC_{cor}$  (Aethalometer;  $\lambda = 590 \text{ nm}$ ) values were  $12.5$  and  $12.7 \text{ m}^2 \text{ g}^{-1}$  for the 1-h and 24-h data, respectively. The  $MAC_{med}$  values of the  $b_{abs}$  (Aethalometer) /  $M_{BC}$  (COSMOS) ratios were  $13.5 \text{ m}^2 \text{ g}^{-1}$  and  $13.8 \text{ m}^2 \text{ g}^{-1}$  for the 1-h and 24-h data, respectively (Fig. 5c and d), which agree with the  $MAC_{cor}$  values to within 8 %. Therefore, depending on the MAC values used, the estimated  $M_{BC}$  values can differ by about 8 %. Because the interquartile ranges of the  $b_{abs}$  (Aethalometer) /  $M_{BC}$  (COSMOS) ratios were  $11.4$ – $16.5 \text{ m}^2 \text{ g}^{-1}$  (1-h data) and  $12.1$ – $15.7 \text{ m}^2 \text{ g}^{-1}$  (24-h data), the  $V_{MAC}$  was about 22% (with an  $M_{BC}$  threshold of  $2 \text{ ng m}^{-3}$ ) for  $b_{abs}$  (Aethalometer;  $\lambda = 590 \text{ nm}$ ) at Alert (Table 3).

The  $MAC_{cor}$  (Aethalometer) values for each wavelength are summarized in Table 4. Note that these wavelength-dependent  $MAC_{cor}$  values should be interpreted as the simple conversion factors to obtain average  $M_{BC}$  from  $b_{abs}$  (Aethalometer), which might have been contributed to by BC and also other light-absorbing aerosols. In other words, these  $MAC_{cor}$  values differ from  $MAC_{BC}$ , as discussed in Sect. 1. The  $r^2$  values were generally high for all wavelengths examined. This weak dependence on wavelength indicates that the contribution of other light-absorbing aerosols such as brown carbon (BrC) to  $b_{abs}$  (Aethalometer) is small or the BrC/BC concentration ratio was rather stable at Alert during 2018–2019, because BrC should enhance light absorption in near ultraviolet wavelengths.

The  $MAC_{cor}$  (Aethalometer) and  $MAC_{cor}$  (PSAP) are compared in Table 5. They agree within 10 % at three wavelengths, despite the different particle size cuts of the inlets for Aethalometer (total suspended particle) and PSAP ( $PM_{10}$ ). This agreement is consistent with the results by Backman et al. (2017), who



showed that the correction factor  $C_f$  of 3.45 for Aethalometer harmonizes  $b_{\text{abs}}$  (Aethalometer) with  $b_{\text{abs}}$  (PSAP),  $b_{\text{abs}}$  (CLAP), and  $b_{\text{abs}}$  (MAAP) at Arctic sites.

### 3.2 Ny-Ålesund

#### 3.2.1 COSMOS-PSAP comparison

440 Simultaneous measurements of  $M_{\text{BC}}$  (COSMOS) for  $\text{PM}_{10}$  and  $b_{\text{abs}}$  (PSAP) for  $\text{PM}_{10}$  began at Ny-Ålesund in 2012 (Sinha et al., 2017; Fig. S2 in the Supplement). The 1-h and 24-h averaged  $b_{\text{abs}}$  (PSAP;  $\lambda = 550$  nm) were well correlated ( $r^2 = 0.76$ – $0.82$ ) with  $M_{\text{BC}}$  (COSMOS), and the  $\text{MAC}_{\text{cor}}$  (PSAP) value for the whole period was  $14.4$ – $15.2$   $\text{m}^2 \text{g}^{-1}$  (Fig. 6a and b). Year-to-year variations of  $\text{MAC}_{\text{cor}}$  (PSAP) are also shown in Fig. 7a and Table 6. The correlation between  $b_{\text{abs}}$  (PSAP) and  $M_{\text{BC}}$  (COSMOS) during  
445 April–December 2012 was weak for unknown reasons. Excluding this period, average  $\text{MAC}_{\text{cor}}$  (PSAP) during 2013–2016 was  $15.2 \pm 2.2$  ( $1\sigma$ ) and  $16.6 \pm 1.4$   $\text{m}^2 \text{g}^{-1}$  for the 1-h and 24-h data, respectively. Although the reason for the relatively large change in  $\text{MAC}_{\text{cor}}$  (PSAP) values during 2014–2015 (Fig. 7a and Table 6) is not clear, this may be partly because  $b_{\text{abs}}$  (PSAP) data from December 2014 to April 2015 (during an “Arctic haze” period) were not available (Fig. S2).

450 The  $\text{MAC}_{\text{med}}$  values of the  $b_{\text{abs}}$  (PSAP) /  $M_{\text{BC}}$  (COSMOS) ratios were  $16.7$  and  $17.2$   $\text{m}^2 \text{g}^{-1}$  for the 1-h and 24-h data, respectively, when the  $M_{\text{BC}}$  threshold of  $2$   $\text{ng m}^{-3}$  was applied in the analysis (Fig. 6c and d). The  $\text{MAC}_{\text{med}}$  values were by  $16$  % and  $13$  % higher than  $\text{MAC}_{\text{cor}}$  for 1-h and 24-h data, respectively (Table 3). Therefore, conversion of  $b_{\text{abs}}$  (PSAP;  $\lambda = 550$  nm) to  $M_{\text{BC}}$  using a constant  $\text{MAC}_{\text{cor}}$  may result in a slightly biased  $M_{\text{BC}}$ , especially for lower  $b_{\text{abs}}$  data. This is partly because the correlation of  $b_{\text{abs}}$   
455 (PSAP) with  $M_{\text{BC}}$  (COSMOS) is not very high and scatter of the data, especially those with lower  $M_{\text{BC}}$  values, contributes to large variations of the  $b_{\text{abs}}$  (PSAP) /  $M_{\text{BC}}$  (COSMOS) ratios (Fig. 6). The interquartile range of the ratios were  $10.6$ – $21.7$   $\text{m}^2 \text{g}^{-1}$  and  $11.9$ – $21.4$   $\text{m}^2 \text{g}^{-1}$  for the 1-h and 24-h data, respectively. Although these large variations might be partly attributed to actual variations in mixing states of BC, artifacts of  $b_{\text{abs}}$  measurements by PSAP at Ny-Ålesund may be a contributing factor,  
460 considering the higher correlations of  $b_{\text{abs}}$  (Aethalometer) at Ny-Ålesund with  $M_{\text{BC}}$  (COSMOS) (Sect. 3.2.2.). Based on the interquartile ranges of the  $b_{\text{abs}}$  (PSAP) /  $M_{\text{BC}}$  (COSMOS) ratios,  $V_{\text{MAC}}$  was about  $35$  % for  $b_{\text{abs}}$  (PSAP;  $\lambda = 550$  nm) at Ny-Ålesund (Table 3). The above-mentioned bias leads to an additional uncertainty of about  $15$  % for the estimates of  $M_{\text{BC}}$ , if the constant  $\text{MAC}_{\text{cor}}$  value is used.

#### 3.2.2 COSMOS-Aethalometer comparison

465 Measurements of  $b_{\text{abs}}$  (Aethalometer;  $\lambda = 590$  nm) for  $\text{PM}_{10}$  were compared with measurements of  $M_{\text{BC}}$  (COSMOS) for  $\text{PM}_{10}$  during 2012–2019. The time series data of  $b_{\text{abs}}$  (Aethalometer;  $\lambda = 590$  nm) were highly correlated with those for  $M_{\text{BC}}$  (COSMOS) (Fig. S3 in the Supplement) ( $r^2 = 0.90$  for both the 1-h and 24-h data; Fig. 8a and b). The  $\text{MAC}_{\text{cor}}$  (Aethalometer;  $\lambda = 590$  nm) values were  $10.2$  and  $10.1$   $\text{m}^2 \text{g}^{-1}$  for the 1-h and 24-h data, respectively. Year-to-year variations of  $\text{MAC}_{\text{cor}}$  (Aethalometer) are also



470 shown in Fig. 7a and Table 7. The  $r^2$  values were generally high for each year and the average  $MAC_{cor}$  (Aethalometer) during 2012–2019 was  $10.2 \pm 1.6$  ( $1\sigma$ ) and  $10.0 \pm 1.3$   $m^2 g^{-1}$  for the 1-h and 24-h data, respectively. The  $MAC_{cor}$  (Aethalometer) value for 2012 was  $8.7$   $m^2 g^{-1}$  at  $590$  nm (i.e.,  $9.3$   $m^2 g^{-1}$  at  $550$  nm assuming the  $\lambda^{-1}$  relationship) for 24-h data, which is consistent with the  $MAC_{cor}$  of  $9.8$   $m^2 g^{-1}$  at  $550$  nm inferred from the SP2 and Aethalometer measurements in the spring of 2012 (Zanatta et al.,  
475 2018). At Ny-Ålesund, the  $MAC_{cor}$  (Aethalometer) values ( $10.2$  and  $10.1$   $m^2 g^{-1}$  for the 1-h and 24-h data, respectively) were systematically lower than the  $MAC_{cor}$  (PSAP) values ( $14.4$   $m^2 g^{-1}$  and  $15.2$   $m^2 g^{-1}$ ). This discrepancy is different from that at Alert (Sect. 3.1.3) and the reason is unclear, but could be partly due to uncertainty in the absolute values of  $b_{abs}$ , as discussed in Sect. 1 and Sect. 2.2.3.

The  $MAC_{med}$  values of the  $b_{abs}$  (Aethalometer) /  $M_{BC}$  (COSMOS) ratios were  $11.2$  and  $12.3$   $m^2 g^{-1}$  for  
480 the 1-h and 24-h data, respectively (Fig. 8c and d). While the  $MAC_{med}$  for the 1-h data agree with  $MAC_{cor}$  to within 10%, there is a 22 % discrepancy for the 24-h data under the assumed threshold setting ( $2$   $ng m^{-3}$ ) of  $M_{BC}$  (COSMOS) (Table 3). Therefore, conversion of 24-h averaged  $b_{abs}$  (Aethalometer;  $\lambda = 590$  nm) to  $M_{BC}$  using a constant  $MAC_{cor}$  may be somewhat biased, especially for lower  $b_{abs}$  values. At Ny-Ålesund, the  $V_{MAC}$  was about 25 % for  $b_{abs}$  (Aethalometer;  $\lambda = 590$  nm). The  
485 above-mentioned bias leads to an additional uncertainty of about 20 % for conversion of 24-averaged low  $b_{abs}$  data to  $M_{BC}$ , if the constant  $MAC_{cor}$  value is assumed.

### 3.3 Barrow

#### 3.3.1 COSMOS-PSAP/CLAP comparison

Simultaneous measurements of  $PM_{10}$  for  $M_{BC}$  (COSMOS) and  $b_{abs}$  (PSAP/CLAP) began at Barrow in  
490 2012 (Sinha et al., 2017). At Barrow, both the PSAP and CLAP aspirated ambient air using  $PM_{10}$  and  $PM_{10}$  impactors alternately for 30 min of each hour. Here we used the data from the PSAP/CLAP equipped with the  $PM_{10}$  impactor and data from the PSAP in 2012–2015 and the CLAP in 2016–2019 (Fig. S4 in the Supplement). Because the 24-h averaged  $b_{abs}$  (PSAP) and  $b_{abs}$  (CLAP) values agreed to within 2 % during 2012–2015 (Sinha et al., 2017) when the PSAP and CLAP overlapped, we consider  
495 the two instruments to be equivalent. The  $M_{BC}$  (COSMOS) data from June 2018 to May 2019 were unavailable due to problems with the COSMOS instrument.

The  $b_{abs}$  (PSAP/CLAP;  $\lambda = 550$  nm) data were strongly correlated with those for  $M_{BC}$  (COSMOS) ( $r^2 = 0.88$  and  $r^2 = 0.86$ ; Fig. 9a and b) and the  $MAC_{cor}$  (PSAP/CLAP) derived from 1-h and 24-h averaged data for the whole period were  $10.8$  and  $10.6$   $m^2 g^{-1}$ , respectively. Average  $MAC_{cor}$  (PSAP/CLAP)  
500 during 2012–2018 was stable at  $11.0 \pm 0.9$  ( $1\sigma$ )  $m^2 g^{-1}$  (Fig. 7b and Table 8). Yearly  $M_{BC}$  (COSMOS) values did not exhibit large changes during this period (Fig. 7b). The  $b_{abs}$  (CLAP) data was weakly correlated with  $M_{BC}$  (COSMOS) data during June–December 2019 (Table 8), indicating that either the CLAP or COSMOS results might not have been accurate during this period. Therefore, in Table 8 we



calculated the average  $MAC_{cor}$  (PSAP/CLAP) by excluding the MAC value for 2019.

505 The  $MAC_{med}$  values of the  $b_{abs}$  (PSAP/CLAP) /  $M_{BC}$  (COSMOS) ratios were 11.2 and 11.0  $m^2 g^{-1}$  for 1-h and 24-h data (Fig. 9c and d), which are very close to the  $MAC_{cor}$  values of 10.8 and 10.6  $m^2 g^{-1}$ , respectively (Table 3). Therefore, when either  $MAC_{cor}$  or  $MAC_{med}$  is used for conversion of  $b_{abs}$  (PSAP/CLAP;  $\lambda = 550$  nm) to  $M_{BC}$ , the resulting  $M_{BC}$  values differ by only about 4 %. The  $V_{MAC}$  was about 25 % for  $b_{abs}$  (PSAP /CLAP;  $\lambda = 550$  nm) at Barrow (Table 3).

## 510 3.4 Pallas

### 3.4.1 COSMOS-MAAP comparison

Measurements of  $b_{abs}$  (MAAP;  $\lambda = 637$  nm) have been made since 2007 at the Global Atmospheric Watch (GAW) station at Pallas (Hyvärinen et al., 2011).  $PM_{10}$  and  $PM_1$  inlets were used for MAAP and COSMOS, respectively.  $M_{BC}$  (COSMOS) measurements began in July 2019; we used the data collected  
515 up to July 2020 in this study. The  $M_{BC}$  (COSMOS) data for about 3 months (February to April 2020) were unavailable due to an air sampling problem.

The  $b_{abs}$  (MAAP) 1-h and 24-h values (Fig. S5 in the Supplement) were strongly correlated with those for  $M_{BC}$  (COSMOS) with  $r^2 = 0.93$  and  $r^2 = 0.95$ , respectively (Fig. 10a and b).  $MAC_{cor}$  (MAAP) was 13.0  $m^2 g^{-1}$  for both the 1-h and 24-h data. This  $MAC_{cor}$  value is about twice the manufacturer's default  
520 setting (= 6.6  $m^2 g^{-1}$ ) of MAC (MAAP). One possible reason is the difference of the methods of  $M_{BC}$  measurements to determine  $MAC_{cor}$  (MAAP) values, as mentioned in Sect. 2.2.3.3. Another reason could be that the difference in microphysical properties of BC (mixing states and size distribution) and properties of co-existing LSPs lead to the different  $MAC_{cor}$  (MAAP) values.

The  $MAC_{med}$  values of the  $b_{abs}$  (MAAP) /  $M_{BC}$  (COSMOS) ratios for the 1-h and 24-h data were 12.4  
525 and 13.1  $m^2 g^{-1}$ , respectively (Fig. 10c and d), which are very close to that for  $MAC_{cor}$  (13.0  $m^2 g^{-1}$  for both 1-h and 24-h data, Table 3). Therefore, the difference between the estimated  $M_{BC}$  values is less than 5 % when these  $MAC_{cor}$  or  $MAC_{med}$  values are used for conversion of  $b_{abs}$  (MAAP) to  $M_{BC}$ . The  $V_{MAC}$  was about 25 % for  $b_{abs}$  (MAAP) at Pallas (Table 3).

## 3.5 Fukue Island

### 530 3.5.1 COSMOS-SP2 comparison

The UT-SP2 was operated at Fukue for 3 weeks in April 2019 (Yoshida et al., 2020), as mentioned in Sect. 2.2.1. Fig. 11a shows the number and mass size distributions of BC measured by the UT-SP2 averaged over the observation period. In addition to the  $M_{BC}$  (SP2) derived by integrating the mass size distributions over the detectable diameter range ( $D_m = 70$ –850 nm), we also estimated  $M_{BC}$  (SP2) in the  
535  $D_m = 30$ –1000 nm range by fitting a lognormal function to the data. As the two sets of  $M_{BC}$  (SP2) values deviated by less than 2 %, we used the former  $M_{BC}$  (SP2) for comparison with  $M_{BC}$  (COSMOS). The



time series of hourly values of  $M_{BC}$  (COSMOS) were strongly correlated ( $r^2 = 0.97$ ) with  $M_{BC}$  (SP2) (Fig. 11b) and the slope of the regression was 0.92 (Fig. 11c). This relationship agrees with those observed by Ohata et al. (2019) at Tokyo, Hedo, and Ny-Ålesund and those observed at Alert (Sect. 3.1.1), thus confirming the clear and consistent relationship between  $M_{BC}$  (COSMOS) and  $M_{BC}$  (SP2). Miyakawa et al. (2017) also reported a strong correlation ( $r^2 = 0.92$ ; regression slope 1.14) between  $M_{BC}$  (COSMOS) and  $M_{BC}$  (SP2) at Fukue in spring 2015 by using an SP2 maintained and calibrated by the Japan Agency for Marine-Earth Science and Technology.

### 3.5.2 COSMOS-MAAP comparison

Kanaya et al. (2013, 2016, 2020) made simultaneous measurements of  $M_{BC}$  (COSMOS) and  $b_{abs}$  (MAAP;  $\lambda = 639$  nm) at Fukue for about 10 years (April 2009–May 2019; Fig. S6 in the Supplement). The air inlet for the MAAP and COSMOS was equipped with a  $PM_{10}$  cyclone after November 2011. Before that a  $PM_{2.5}$  cyclone was used instead.  $b_{abs}$  (MAAP) was highly correlated ( $r^2 = 0.94$ ) with  $M_{BC}$  (COSMOS) and the  $MAC_{cor}$  (MAAP) for the entire period was found to be  $10.8$   $m^2$   $g^{-1}$  and  $10.9$   $m^2$   $g^{-1}$  for the 1-h and 24-h data (Fig. 12a and b), respectively. Because the correlation of  $b_{abs}$  (MAAP) with  $M_{BC}$  (COSMOS) was also strong for individual years,  $MAC_{cor}$  (MAAP) for each year was also derived (Fig. 7c and Table 9).  $M_{BC}$  (COSMOS) decreased by about 50 % during this period, owing to a large decrease of BC emissions in China (Kanaya et al., 2020). However, the yearly average  $MAC_{cor}$  (MAAP) values were stable at  $11.1 \pm 1.0$  ( $1\sigma$ )  $m^2$   $g^{-1}$  for both the 1-h and 24-h data, despite the large change in  $M_{BC}$  (COSMOS). This  $MAC_{cor}$  value is considerably higher than the manufacturer's default setting ( $= 6.6$   $m^2$   $g^{-1}$ ), possibly for the same reasons discussed in Sect. 3.4.1.

Because the number of data with  $M_{BC}$  less than  $2$   $ng$   $m^{-3}$  was very small at Fukue, the  $MAC_{med}$  values and the interquartile ranges of the  $b_{abs}$  (MAAP) /  $M_{BC}$  (COSMOS) ratios were obtained for all data without applying any threshold of  $M_{BC}$ . The  $MAC_{med}$  was  $11.4$   $m^2$   $g^{-1}$  for both 1-h and 24-h data (Fig. 12c and d), which agrees well (within 6 %) with the  $MAC_{cor}$  values derived from correlation plots ( $10.8$  and  $10.9$   $m^2$   $g^{-1}$  for 1-h and 24-h data, respectively) (Table 3). Therefore, using either  $MAC_{cor}$  or  $MAC_{med}$  for conversion of  $b_{abs}$  (MAAP) to  $M_{BC}$  affects the resulting  $M_{BC}$  values by less than 6 %. The  $V_{MAC}$  was about 15 %, which is lower than those at Arctic sites (Table 3) partly because the higher  $M_{BC}$  (COSMOS) values at Fukue make the calculated ratios more stable. Also, aerosol properties including mixing states of BC might be more stable at Fukue than those at the Arctic sites examined in this study.

### 3.6 Spatial variability of $MAC_{cor}$ and $r^2$

In previous sections, we showed that the  $MAC_{cor}$  values depended on instrument and observation site. The values of  $MAC_{cor}$  ( $\lambda = 550$  nm) and  $r^2$  are summarized in Table 10. Here, the  $MAC_{cor}$  (MAAP;  $\lambda \sim 637$  nm) and  $MAC_{cor}$  (Aethalometer;  $\lambda = 590$  nm) values were adjusted to those at  $\lambda = 550$  nm by





570 assuming an absorption Ångström exponent of 1.0 (i.e., a  $\lambda^{-1}$  relationship). The unit-to-unit variations of  
 $b_{\text{abs}}$  measurements were reported to be within 5 % for MAAP (Müller et al., 2011), 6 % for PSAP (Bond  
et al., 1999), and 4 % for CLAP (Ogren et al., 2017), if the careful calibration of flows and filter  
sampling spot sizes of these instruments are made for individual units. Therefore, the spatial variations  
of  $\text{MAC}_{\text{cor}}$  values observed in this study likely reflects differences of aerosol properties at the  
575 observation sites.

The values of  $\text{MAC}_{\text{cor}}$  (PSAP) at Alert and  $\text{MAC}_{\text{cor}}$  (PSAP/CLAP) at Barrow were both determined  
with a  $\text{PM}_{10}$  size cut and they differed by about 22 % for 1-h data. Differences in aerosol properties  
including mixing states of BC at these sites could contribute to the different MAC values, although this  
effect cannot be assessed quantitatively with only this dataset. The correlations of  $b_{\text{abs}}$  (PSAP) with  $M_{\text{BC}}$   
580 (COSMOS) at Alert were somewhat higher ( $r^2 = 0.96$ ) than those of  $b_{\text{abs}}$  (PSAP/CLAP) at Barrow ( $r^2 =$   
0.84–0.87). The stronger correlation of  $b_{\text{abs}}$  (PSAP) with  $M_{\text{BC}}$  (COSMOS) at Alert suggests that  
environmental conditions including LSP/BC ratios and mixing states of BC were more stable at Alert.  
We found that at Alert  $b_{\text{abs}}$  (PSAP) data with loading and scattering corrections were strongly correlated  
with the uncorrected  $b_{\text{abs}}$  (PSAP) data and the contribution of the loading and scattering corrections was  
585 about 35 %, on average. In contrast at Barrow, the contribution of these corrections was about 63 %.  
This indicates that at Alert, the LSP/BC ratio was small and stable at Alert, and the influence of LSPs  
on derived  $b_{\text{abs}}$  (PSAP) was small. The greater distance from continental sources of aerosols at Alert  
than at Barrow (Fig. 1), which may contribute to these observed differences.

At Ny-Ålesund, where a  $\text{PM}_{10}$  inlet was used, the  $\text{MAC}_{\text{cor}}$  (PSAP) values were higher than those at  
590 Alert and Barrow. Also, the  $r^2$  values at Ny-Ålesund ( $r^2 = 0.84$ –0.89) were lower than those at Alert.  
Effects of particles larger than 1  $\mu\text{m}$  including dust and sea salt may partly contribute to the larger MAC  
and lower  $r^2$  values at Ny-Ålesund.

The  $\text{MAC}_{\text{cor}}$  (PSAP) and  $\text{MAC}_{\text{cor}}$  (Aethalometer) agree to within 4 % for 1-h data at Alert, in spite of  
the different particle size cut of the inlets. However, they differed by about 24% for 1-h data at Ny-  
595 Ålesund. Although the agreements were somewhat better for 2015–2016 at Ny-Ålesund (Fig. 7a), the  
reason for the overall discrepancy is unknown. Furthermore, while the  $\text{MAC}_{\text{cor}}$  (PSAP) at Ny-Ålesund  
was higher than that at Alert, the opposite result was obtained by Aethalometers, which is not easily  
interpreted.

The values of  $\text{MAC}_{\text{cor}}$  (MAAP) determined at Pallas and Fukue differ by about 17%. This difference  
600 may be attributed to the difference of average mixing states of BC and properties of other co-existing  
aerosols, which were affected by environmental conditions and also by the different particle size cuts  
used at these sites (i.e.,  $\text{PM}_{10}$  for Fukue and  $\text{PM}_{10}$  for Pallas). Because these are the only available  
 $\text{MAC}_{\text{cor}}$  (MAAP) data sets derived from  $M_{\text{BC}}$  (COSMOS), it is difficult to further evaluate spatial  
variability.





605 We have shown that in general,  $b_{\text{abs}}$  values obtained by PSAP, CLAP, Aethalometer, and MAAP were strongly correlated with  $M_{\text{BC}}$  (COSMOS) at all four Arctic sites, although the strength of the correlations differed somewhat among the sites. Based on the analysis of  $b_{\text{abs}}/M_{\text{BC}}$  variations among these sites, the  $\text{MAC}_{\text{cor}}$  and  $\text{MAC}_{\text{med}}$  were most stable for PSAP with a  $\text{PM}_{10}$  inlet at Alert and most variable for PSAP with a  $\text{PM}_{10}$  inlet at Ny-Ålesund (Table 3). The average  $\text{MAC}_{\text{cor}}$  ( $\lambda = 550$  nm) values  
610 at these four Arctic sites were  $13.1 \pm 1.7$  ( $1\sigma$ ; 13 % of the average) and  $13.2 \pm 1.9$  ( $1\sigma$ ; 14 %)  $\text{m}^2 \text{g}^{-1}$  for 1-h and 24-h data, respectively (Table 10). However, these correlations and resulting  $\text{MAC}_{\text{cor}}$  values may not hold outside the Arctic, where environmental conditions can be very different, especially the mixing states of BC and amount of interference by LSPs.

Zanatta et al. (2016), using  $M_{\text{EC}}$  measured by the thermal-optical transmittance method with the  
615 EUSAAR-2 protocol instead of  $M_{\text{BC}}$  (COSMOS), reported the average  $\text{MAC}_{\text{cor}}$  value at  $\lambda = 637$  nm for nine European background sites to be  $10.0 \text{ m}^2 \text{g}^{-1}$ . From this  $\text{MAC}_{\text{cor}}$  ( $\lambda = 637$  nm) value, the value of  $\text{MAC}_{\text{cor}}$  at  $\lambda = 550$  nm is calculated to be  $11.6 \text{ m}^2 \text{g}^{-1}$  by assuming an absorption Ångstrom exponent of 1.0. Although their  $\text{MAC}_{\text{cor}}$  values were generally obtained using  $\text{PM}_{10}$  inlets or without particle size-cuts, their average  $\text{MAC}_{\text{cor}}$  value ( $= 11.6 \text{ m}^2 \text{g}^{-1}$ ) is about 15 % lower than our average  $\text{MAC}_{\text{cor}}$  value  
620 ( $13.1\text{--}13.2 \text{ m}^2 \text{g}^{-1}$ ) at 4 Arctic sites determined in this study. This discrepancy may be partly due to the different methods used to determine absolute mass concentrations of BC.

Mason et al. (2018) derived the values of  $\text{MAC}_{\text{cor}}$  (PSAP) and  $\text{MAC}_{\text{cor}}$  (CLAP) for  $\text{PM}_{10}$  size range in biomass burning and agriculture fire plumes during the SEAC<sup>4</sup>RS aircraft observation campaign by using  $M_{\text{BC}}$  (SP2) data. They reported the  $\text{MAC}_{\text{cor}}$  (PSAP;  $\lambda = 532$  nm) and  $\text{MAC}_{\text{cor}}$  (CLAP;  $\lambda = 532$  nm)  
625 values to be  $21.0$  and  $26.5 \text{ m}^2 \text{g}^{-1}$ , respectively, which are about 60 % larger than the average  $\text{MAC}_{\text{cor}}$  value ( $13.1\text{--}13.2 \text{ m}^2 \text{g}^{-1}$ ) determined in this study. Although the causes for their very high  $\text{MAC}_{\text{cor}}$  values are not clear, one possible explanation given by Mason et al. (2018) is the considerable amount of additional absorbers other than BC, including tar balls, that might have existed in their samples. Also, strong lensing effects by BC coatings could contribute to the high  $\text{MAC}_{\text{cor}}$  values. Thus, the  $\text{MAC}_{\text{cor}}$   
630 values can be highly dependent on environmental conditions and those reported in the present study are considered to be site-specific values, although the variability ( $1\sigma$ ) of our  $\text{MAC}_{\text{cor}}$  values in the 4 Arctic sites was within 14% of the average  $\text{MAC}_{\text{cor}}$  value for these 4 sites.

#### 4 Summary and conclusions

Long-term measurements of  $M_{\text{BC}}$  by ground-based instruments are needed to investigate changes in the  
635 emission, transport, and deposition of BC. Various types of filter-based absorption photometers, including the particle absorption soot photometer (PSAP), the continuous light absorption photometer (CLAP), the Aethalometer, and the multi-angle absorption photometer (MAAP) have been used in the Arctic. To date, the accuracy of  $M_{\text{BC}}$  estimated from absorption coefficients ( $b_{\text{abs}}$ ) measured by these



instruments have not been adequately assessed, mainly because of a lack of simultaneous and reliable  
640  $M_{BC}$  measurements.

In this paper, we introduced a systematic methodology to derive  $M_{BC}$  from  $b_{abs}$  measured by these  
instruments. To obtain accurate values of  $M_{BC}$ , we used a filter-based absorption photometer with a  
heated inlet (COSMOS), which we calibrated to within 10 % uncertainty with an SP2 deployed in  
Tokyo. Individual COSMOS instruments used for field observations were calibrated against the  
645 standard COSMOS to within about 10 %. The accuracy of  $M_{BC}$  (COSMOS) has previously been  
demonstrated to be about 15 % by comparison with  $M_{BC}$  (SP2) in Asia and the Arctic. The effect on  
 $M_{BC}$  (COSMOS) of interference by light-absorbing  $FeO_x$  particles was estimated to be only a few  
percent, owing partly to the particle-size cut off of 1  $\mu m$  by the  $PM_{10}$  cyclone used. This effect may be  
somewhat higher for the other filter-based absorption photometers equipped with larger particle-size  
650 cuts. The two necessary conditions for application of our method are a high correlation of  $b_{abs}$  with  
independently measured  $M_{BC}$  and long-term stability of the slope of the regression, which represents  
 $MAC_{cor}$ .

We compared  $b_{abs}$  (PSAP/CLAP) with  $M_{BC}$  (COSMOS) at Alert ( $PM_{10}$ ) for 2 years, Ny-Ålesund ( $PM_{10}$ )  
for 4 years, and Barrow ( $PM_{10}$ ) for 7 years. The  $b_{abs}$  (PSAP/CLAP) was highly correlated with  $M_{BC}$   
655 (COSMOS) at these sites. For 1-h data, the  $MAC_{cor}$  (PSAP/CLAP) at  $\lambda = 550$  nm was  $13.9$   $m^2$   $g^{-1}$  at  
Alert,  $14.4$   $m^2$   $g^{-1}$  at Ny-Ålesund, and  $10.8$   $m^2$   $g^{-1}$  at Barrow. The  $V_{MAC}$  was 19 % at Alert, 37 % at Ny-  
Ålesund, and 22 % at Barrow (Table 3).

We also compared  $b_{abs}$  (Aethalometer) with  $M_{BC}$  (COSMOS) at Alert (total suspended particles) for 2  
years and at Ny-Ålesund ( $PM_{10}$ ) for 8 years. They were highly correlated and the  $MAC_{cor}$   
660 (Aethalometer) at  $\lambda = 590$  nm for 1-h data was  $12.5$   $m^2$   $g^{-1}$  at Alert and  $10.2$   $m^2$   $g^{-1}$  at Ny-Ålesund. The  
 $V_{MAC}$  was 22 % at Alert and 25 % at Ny-Ålesund (Table 3).

The  $b_{abs}$  (MAAP) and  $M_{BC}$  (COSMOS) were also compared at Pallas ( $PM_{10}$ ) for about 1 year and at  
Fukue ( $PM_{10}$ ) for about 10 years.  $b_{abs}$  (MAAP) was highly correlated with  $M_{BC}$  (COSMOS) at these sites.  
The  $MAC_{cor}$  (MAAP) at  $\lambda = 637$  nm was  $13.0$   $m^2$   $g^{-1}$  at Pallas for both 1-h and 24-h data. The  $MAC_{med}$   
665 (MAAP) at  $\lambda = 639$  nm at Fukue was stable at  $11.1 \pm 1.0$   $m^2$   $g^{-1}$ , despite a 50 % decrease in  $M_{BC}$   
(COSMOS) during this period (Table 3). The default setting of  $MAC_{cor}$  (MAAP) by the manufacturer  
( $6.6$   $m^2$   $g^{-1}$ ) is about half the present values, indicating a similar overestimation of  $M_{BC}$  if the default  
value is used to convert  $b_{abs}$  (MAAP) to  $M_{BC}$  at these sites. The  $V_{MAC}$  was 25 % at Pallas and 15 % at  
Fukue.

670 Our results show that  $M_{BC}$  can be derived from  $b_{abs}$  obtained from PSAP, CLAP, Aethalometer, and  
MAAP measurements with reasonable accuracy by using the  $MAC_{cor}$  obtained from the regression  
slope of the  $b_{abs}$ - $M_{BC}$  correlation, especially for long data-averaging times. However, scatter in  $b_{abs}$ -



$M_{BC}$  (COSMOS) correlations indicate that the accuracy of this method will be somewhat lower than that achieved by direct measurement of  $M_{BC}$  (COSMOS). We also caution that the reliability of the use of  
675  $b_{abs}$  data to derive  $M_{BC}$  at other locations, especially those outside the Arctic, is unknown. Rigorous comparisons with COSMOS or SP2 data, such as those of this study, are required if use of our method is to expand beyond the Arctic region. Moreover, long-term comparisons are desirable for accurate determination of the  $MAC_{cor}$ . Short-term comparisons will be of limited value for understanding the variability of MAC for each instrument and location.

#### 680 **Data availability**

The observational data set used in this publication is available online (<https://ads.nipr.ac.jp/dataset/A20201120-001>).

#### **Author contributions**

SO, TM, and YKo designed the study, conducted the analyses, and wrote the paper. SS and DV  
685 contributed to the field observations and data analysis of SP2, PSAP, CLAP, and Aethalometer at Alert. AH, EAs, JB, and HS contributed to the field observations and data analysis of MAAP at Pallas. EAn contributed to the field observations and data analysis of PSAP and CLAP at Barrow. PT obtained and analyzed PSAP data at Ny-Ålesund. KE and SV obtained and analyzed Aethalometer data at Ny-Ålesund. YKa contributed to the field observations and data analysis of MAAP and COSMOS at Fukue.  
690 AY and NM obtained and analyzed SP2 data at Fukue. SO, TM, YKo, MK, YZ, YT, JM, and NO contributed to instrument maintenance and data analysis of COSMOS.

#### **Competing interests**

The authors declare that they have no conflicts of interest.

#### **Acknowledgements**

695 We thank Kevin Rawlings and Melody Fraser of Environment and Climate Change (Canada) and CFS Alert for operations and maintenance of the Alert site. We thank Bryan Thomas, Peter Detwiler, and Ross Peterson for supporting the measurements at Barrow. We thank the staff of the Norwegian Polar Institute for supporting the measurements at Ny-Ålesund (Zeppelin). This research was performed by the Environment Research and Technology Development Fund (JPMEERF20142003,  
700 JPMEERF20172003, JPMEERF20202003, and JPMEERF20205001) of the Environmental Restoration and Conservation Agency of Japan; the Japanese Ministry of Education, Culture, Sports, Science, and Technology; the Japan Society for the Promotion of Science KAKENHI Grants (JP12J06736,



JP1604452, JP23221001, JP26241003, JP26701004, JP16H01770, JP17H04709, JP18H03363,  
JP19K20437, JP19K20441, and JP20H00638); the Arctic Challenge for Sustainability (ArCS) project  
705 (JPMXD1300000000); the Arctic Challenge for Sustainability II (ArCS II) project  
(JPMXD1420318865); and a grant for the Global Environmental Research Coordination System from  
the Ministry of the Environment, Japan (MLIT1753). Pallas and Zeppelin measurements and/or analysis  
were conducted under the financial support of the ACTRIS by the European Union's Horizon 2020  
research and innovation programme under grant agreement no. 654109, partly under the European  
710 Union's Horizon 2020 research and innovation program under grant agreement no. 689443 via project  
iCUPE (Integrative and Comprehensive Understanding on Polar Environments) and the 16ENV02  
Black Carbon project of the European Union through the European Metrology Programme for  
Innovation and Research (EMPIR). The research was also supported by Academy of Finland via project  
NABCEA (grant no. 29664) and Academy of Finland Flagship funding (grant no. 337552). E. Andrews  
715 contribution to this effort was supported in part by the Atmospheric Radiation Measurement (ARM)  
user facility, a US Department of Energy (DOE) Office of Science user facility managed by the  
Biological and Environmental Research program.

## References

- Arctic Monitoring and Assessment Programme (AMAP): AMAP Assessment 2015: Black carbon and  
720 ozone as Arctic climate forcers, Oslo, Norway, pp. vii + 116, 2015.
- Asmi, E., Backman, J., Servomaa, H., Virkkula, A., Gini, M., Eleftheriadis, K., Müller, T., Ohata, S.,  
Kondo, Y., and Hyvärinen, A.: Characterizing the Arctic absorbing aerosol with multi-instrument  
observations, *Atmos. Meas. Tech. Discuss.*, <https://doi.org/10.5194/amt-2020-400>, 2020.
- Backman, J., Schmeisser, L., Virkkula, A., Ogren, J. A., Asmi, E., Starkweather, S., Sharma, S.,  
725 Eleftheriadis, K., Uttal, T., Jefferson, A., Bergin, M., Makshtas, A., Tunved, P., and Fiebig, M.:  
On Aethalometer measurement uncertainties and an instrument correction factor for the Arctic,  
*Atmos. Meas. Tech.*, 10, 5039–5062, <https://doi.org/10.5194/amt-10-5039-2017>, 2017.
- Baumgardner, D., Popovicheva, O., Allan, J., Bernardoni, V., Cao, J., Cavalli, F., Cozic, J., Diapouli, E.,  
Eleftheriadis, K., Genberg, P. J., Gonzalez, C., Gysel, M., John, A., Kirchstetter, T. W.,  
730 Kuhlbusch, T. A. J., Laborde, M., Lack, D., Müller, T., Niessner, R., Petzold, A., Piazzalunga, A.,  
Putaud, J. P., Schwarz, J., Sheridan, P., Subramanian, R., Swietlicki, E., Valli, G., Vecchi, R., and  
Viana, M.: Soot reference materials for instrument calibration and intercomparisons: A workshop  
summary with recommendations, *Atmos. Meas. Tech.*, 5, 1869–1887,  
<https://doi.org/10.5194/amt-5-1869-2012>, 2012.
- 735 Bellouin, N., Quaas, J., Gryspeerdt, E., Kinne, S., Stier, P., Watson-Parris, D., Boucher, O., Carslaw, K.  
S., Christensen, M., Daniau, A.-L., Dufresne, J.-L., Feinglod, G., Fiedler, S., Foster, P., Gettelman,



- A., Haywood, J. M., Lohmann, U., Malavelle, F., Mauritsen, T., McCoy, D. T., Myhre, G., Mülmenstädt, J., Neubauer, D., Possner, A., Rugenstein, M., Sato, Y., Schulz, M., Schwartz, S. E., Sourdeval, O., Storelvmo, T., Toll, V., Winker, D., and Stevens, B.: Bounding global aerosol radiative forcing of climate change, *Rev. Geophys.*, 58, e2019RG000660, <https://doi.org/10.1029/2019RG000660>, 2020.
- 740 Bergstrom, R. W.: Predictions of the spectral absorption and extinction coefficients of an urban air pollution aerosol model, *Atmos. Environ.*, 6, 247–258, [https://doi.org/10.1016/0004-6981\(72\)90083-2](https://doi.org/10.1016/0004-6981(72)90083-2), 1972.
- 745 Bond, T. C. and Bergstrom, R. W.: Light absorption by carbonaceous particles: An investigative review, *Aerosol Sci. Tech.*, 40, 1, 27–67, <https://doi.org/10.1080/02786820500421521>, 2006.
- Bond, T. C., Anderson, T. L., and Campbell, D.: Calibration and Intercomparison of Filter-Based Measurements of Visible Light Absorption by Aerosols, *Aerosol Sci. Tech.*, 30, 6, 582–600, <https://doi.org/10.1080/027868299304435>, 1999.
- 750 Bond, T. C., Habib, G., and Bergstrom, R. W.: Limitations in the enhancement of visible light absorption due to mixing state, *J. Geophys. Res. Atmos.*, 111, D20211, <https://doi.org/10.1029/2006JD007315>, 2006.
- Bond, T. C., Doherty, S. J., Fahey, D. W., Forster, P. M., Berntsen, T., Deangelo, B. J., Flanner, M. G., Ghan, S., Kärcher, B., Koch, D., Kinne, S., Kondo, Y., Quinn, P. K., Sarofim, M. C., Schultz, M., G., Schulz, M., Venkataraman, C., Zhang, H., Zhang, S., Bellouin, N., Guttikunda, S. K., Hopke, P. K., Jacobson, M. Z., Kaiser, J. W., Klimont, Z., Lohmann, U., Schwarz, J. P., Shindell, D., Storelvmo, T., Warren, S. G., and Zender, C. S.: Bounding the role of black carbon in the climate system: A scientific assessment, *J. Geophys. Res. Atmos.*, 118, 1–173, <https://doi.org/10.1002/jgrd.50171>, 2013.
- 755 G., Schulz, M., Venkataraman, C., Zhang, H., Zhang, S., Bellouin, N., Guttikunda, S. K., Hopke, P. K., Jacobson, M. Z., Kaiser, J. W., Klimont, Z., Lohmann, U., Schwarz, J. P., Shindell, D., Storelvmo, T., Warren, S. G., and Zender, C. S.: Bounding the role of black carbon in the climate system: A scientific assessment, *J. Geophys. Res. Atmos.*, 118, 1–173, <https://doi.org/10.1002/jgrd.50171>, 2013.
- 760 Cho, C., Schwarz, J. P., Perring, A. E., Lamb, K. D., Kondo, Y., Park, J., Park, D., Shim, K., Park, J., Park, R. J., Lee, M., Song, C., and Kim, S.: Science of the Total Environment Light-absorption enhancement of black carbon in the Asian out flow inferred from airborne SP2 and in-situ measurements during KORUS-AQ, *Sci. Total Environ.*, 773, 145531, <https://doi.org/10.1016/j.scitotenv.2021.145531>, 2021.
- 765 Eleftheriadis, K., Vratolis, S., and Nyeki, S.: Aerosol black carbon in the European Arctic: Measurements at Zeppelin station, Ny-Ålesund, Svalbard from 1998–2007, *Geophys. Res. Lett.*, 36, L02809, <https://doi.org/10.1029/2008GL035741>, 2009.
- Eyring, V., Bony, S., Meehl, G. A., Senior, C. A., Stevens, B., Stouffer, R. J., and Taylor, K. E.: Overview of the Coupled Model Intercomparison Project Phase 6 (CMIP6) experimental design



- 770 and organization, *Geosci. Model Dev.*, 9, 1937–1958, <https://doi.org/10.5194/gmd-9-1937-2016>, 2016.
- Flanner, M. G., Zender, C. S., Hess, P. G., Mahowald, N. M., Painter, T. H., Ramanathan, V., and Rasch, P. J.: Springtime warming and reduced snow cover from carbonaceous particles, *Atmos. Chem. Phys.*, 9, 2481–2497, <https://doi.org/10.5194/acp-9-2481-2009>, 2009.
- 775 Gysel, M., Laborde, M., Olfert, J. S., Subramanian, R., and Gréhn, A. J.: Effective density of Aquadag and fullerene soot black carbon reference materials used for SP2 calibration, *Atmos. Meas. Tech.*, 4, 2851–2858, <https://doi.org/10.5194/amt-4-2851-2011>, 2011.
- Hansen, A. D. A., Rosen, H., and Novakov, T.: The aethalometer – an instrument for the real-time measurement of optical absorption by aerosol particles, *Sci. Total Environ.*, 36, 191–196, 1984.
- 780 Huffman, D. R. and Stapp, J. L.: Optical Measurements on Solids of Possible Interstellar Importance, in: *Interstellar dust and related topics*, edited by: Greenberg, J. M. and Van de Hulst, H. C., Reidel, Boston, pp. 297–301, 1973.
- Hyvärinen, A. P., Kolmonen, P., Kerminen, V. M., Virkkula, A., Leskinen, A., Komppula, M., Hatakka, J., Burkhardt, J., Stohl, A., Aalto, P., Kulmala, M., Lehtinen, K. E. J., Viisanen, Y., and Lihavainen, H.: Aerosol black carbon at five background measurement sites over Finland, a gateway to the  
785 Arctic, *Atmos. Environ.*, 45, 4042–4050, <https://doi.org/10.1016/j.atmosenv.2011.04.026>, 2011.
- Irwin, M., Kondo, Y., and Moteki, N.: An empirical correction factor for filter-based photo-absorption black carbon measurements, *J. Aerosol Sci.*, 80, 86–97, <https://doi.org/10.1016/j.jaerosci.2014.11.001>, 2015.
- 790 Kanaya, Y., Taketani, F., Komazaki, Y., Liu, X., Kondo, Y., Sahu, L. K., Irie, H., and Takashima, H.: Comparison of black carbon mass concentrations observed by multi-angle absorption photometer (MAAP) and continuous soot-monitoring system (COSMOS) on Fukue Island and in Tokyo, Japan, *Aerosol Sci. Tech.*, 47, 1, 1–10, <https://doi.org/10.1080/02786826.2012.716551>, 2013.
- Kanaya, Y., Pan, X., Miyakawa, T., Komazaki, Y., Taketani, F., Uno, I., and Kondo, Y.: Long-term  
795 observations of black carbon mass concentrations at Fukue Island, western Japan, during 2009–2015: constraining wet removal rates and emission strengths from East Asia, *Atmos. Chem. Phys.*, 16, 10689–10705, <https://doi.org/10.5194/acp-16-10689-2016>, 2016.
- Kanaya, Y., Yamaji, K., Miyakawa, T., Taketani, F., Zhu, C., Choi, Y., Komazaki, Y., Ikeda, K., Kondo, Y., and Klimont, Z.: Rapid reduction in black carbon emissions from China: Evidence from 2009–  
800 2019 observations on Fukue Island, Japan, *Atmos. Chem. Phys.*, 20, 6339–6356, <https://doi.org/10.5194/acp-20-6339-2020>, 2020.



- Kondo, Y.: Effects of Black Carbon on Climate: Advances in Measurement and Modeling, Monogr. Environ. Earth Planets, 3, 1–85, <https://doi.org/10.5047/meep.2015.00301.0001>, 2015.
- 805 Kondo, Y., Sahu, L., Kuwata, M., Miyazaki, Y., Takegawa, N., Moteki, N., Imaru, J., Han, S., Nakayama, T., Oanh, N. T. K., Hu, M., Kim, Y. J., and Kita, K.: Stabilization of the mass absorption cross section of black carbon for filter-based absorption photometry by the use of a heated inlet, *Aerosol Sci. Tech.*, 43, 8, 741–756, <https://doi.org/10.1080/02786820902889879>, 2009.
- 810 Kondo, Y., Sahu, L., Moteki, N., Khan, F., Takegawa, N., Liu, X., Koike, M., and Miyakawa, T.: Consistency and traceability of black carbon measurements made by laser-induced incandescence, thermal-optical transmittance, and filter-based photo-absorption techniques, *Aerosol Sci. Tech.*, 45, 2, 295–312, <https://doi.org/10.1080/02786826.2010.533215>, 2011.
- 815 Laborde, M., Mertes, P., Zieger, P., Dommen, J., Baltensperger, U., and Gysel, M.: Sensitivity of the Single Particle Soot Photometer to different black carbon types, *Atmos. Meas. Tech.*, 5, 1031–1043, <https://doi.org/10.5194/amt-5-1031-2012>, 2012.
- Lack, D. A., Cappa, C. D., Covert, D. S., Baynard, T., Massoli, P., Sierau, B., Bates, T. S., Quinn, P. K., Lovejoy, E. R., and Ravishankara, A. R.: Bias in filter-based aerosol light absorption measurements due to organic aerosol loading: Evidence from ambient measurements, *Aerosol Sci. Tech.*, 42, 1033–1041, <https://doi.org/10.1080/02786820802389277>, 2008.
- 820 Lamb, K. D.: Classification of iron oxide aerosols by a single particle soot photometer using supervised machine learning, *Atmos. Meas. Tech.*, 12, 3885–3906, <https://doi.org/10.5194/amt-12-3885-2019>, 2019.
- Lihavainen, H., Hyvärinen, A., Asmi, E., Hatakka, J., and Viisanen, Y.: Long-term variability of aerosol optical properties in northern Finland, *Boreal Env. Res.*, 20, 526–541, 2015.
- 825 Mason, B., Wagner, N. L., Adler, G., Andrews, E., Brock, C. A., Gordon, T. D., Lack, D. A., Perring, A. E., Richardson, M. S., Schwarz, J. P., Shook, M. A., Thornhill, K. L., Ziemba, L. D., and Murphy, D. M.: An intercomparison of aerosol absorption measurements conducted during the SEAC<sup>4</sup>RS campaign, *Aerosol Sci. Tech.*, 52, 1012–1027, <https://doi.org/10.1080/02786826.2018.1500012>, 2018.
- 830 Matsui, H., Mahowald, N. M., Moteki, N., Hamilton, D. S., Ohata, S., Yoshida, A., Koike, M., Scanza, R. A., and Flanner, M. G.: Anthropogenic combustion iron as a complex climate forcer, *Nat. Commun.*, 9, <https://doi.org/10.1038/s41467-018-03997-0>, 2018.
- Miyakawa, T., Oshima, N., Taketani, F., Komazaki, Y., Yoshino, A., Takami, A., Kondo, Y., and Kanaya, Y.: Alteration of the size distributions and mixing states of black carbon through





- 835 transport in the boundary layer in east Asia, *Atmos. Chem. Phys.*, 17, 5851–5864,  
<https://doi.org/10.5194/acp-17-5851-2017>, 2017.
- Miyazaki, Y., Kondo, Y., Sahu, L. K., Imaru, J., Fukushima, N., and Kano, M.: Performance of a newly  
designed continuous soot monitoring system (COSMOS), *J. Environ. Monitor.*, 10, 1195–1201,  
<https://doi.org/10.1039/b806957c>, 2008.
- 840 Moosmüller, H., Chakrabarty, R.K., and Arnott, W.P.: Aerosol light absorption and its measurement: A  
review, *J. Quant. Spectrosc. Radiat. Transf.*, 110, 844–878,  
<https://doi.org/10.1016/j.jqsrt.2009.02.035>, 2009.
- Moteki, N. and Kondo, Y.: Dependence of laser-induced incandescence on physical properties of black  
carbon aerosols: Measurements and theoretical interpretation, *Aerosol Sci. Technol.*, 44, 8, 663–  
845 675, <https://doi.org/10.1080/02786826.2010.484450>, 2010.
- Moteki, N., Adachi, K., Ohata, S., Yoshida, A., Harigaya, T., Koike, M., and Kondo, Y.: Anthropogenic  
iron oxide aerosols enhance atmospheric heating, *Nat. Commun.*, 8,  
<https://doi.org/10.1038/ncomms15329>, 2017.
- Müller, T., Henzing, J. S., De Leeuw, G., Wiedensohler, A., Alastuey, A., Angelov, H., Bizjak, M.,  
850 Collaud Coen, M., Engström, J. E., Gruening, C., Hillamo, R., Hoffer, A., Imre, K., Ivanow, P.,  
Jennings, G., Sun, J. Y., Kalivitis, N., Karlsson, H., Komppula, M., Laj, P., Li, S. M., Lunder, C.,  
Marinoni, A., Martins Dos Santos, S., Moerman, M., Nowak, A., Ogren, J. A., Petzold, A., Pichon,  
J. M., Rodriguez, S., Sharma, S., Sheridan, P. J., Teinilä, K., Tuch, T., Viana, M., Virkkula, A.,  
Weingartner, E., Wilhelm, R., and Wang, Y. Q.: Characterization and intercomparison of aerosol  
855 absorption photometers: result of two intercomparison workshops, *Atmos. Meas. Tech.*, 4, 245–  
268, <https://doi.org/10.5194/amt-4-245-2011>, 2011.
- Ogren, J. A.: Comment on “calibration and intercomparison of filter-based measurements of visible  
light absorption by aerosols,” *Aerosol Sci. Tech.*, 44, 8, 589–591,  
<https://doi.org/10.1080/02786826.2010.482111>, 2010.
- 860 Ogren, J. A., Wendell, J., Andrews, E., and Sheridan, P. J.: Continuous light absorption photometer for  
long-term studies, *Atmos. Meas. Tech.*, 10, 4805–4818, [https://doi.org/10.5194/amt-10-4805-  
2017](https://doi.org/10.5194/amt-10-4805-2017), 2017.
- Ohata, S., Yoshida, A., Moteki, N., Adachi, K., Takahashi, Y., Kurisu, M., and Koike, M.: Abundance  
of Light-Absorbing Anthropogenic Iron Oxide Aerosols in the Urban Atmosphere and Their  
865 Emission Sources, *J. Geophys. Res. Atmos.*, 123, 8115–8134,  
<https://doi.org/10.1029/2018JD028363>, 2018.



- Ohata, S., Kondo, Y., Moteki, N., Mori, T., Yoshida, A., Sinha, P. R., and Koike, M.: Accuracy of black carbon measurements by a filter-based absorption photometer with a heated inlet, *Aerosol Sci. Tech.*, 53, 9, 1079–1091, <https://doi.org/10.1080/02786826.2019.1627283>, 2019.
- 870 Oshima, N., Yukimoto, S., Deushi, M., Koshiro, T., Kawai, H., Tanaka, T. Y., and Yoshida, K.: Global and Arctic Radiative Forcing of Anthropogenic Gases and Aerosols in MRI-ESM2.0, *Prog. Earth Planet. Sci.*, 7, 38, <https://doi.org/10.1186/s40645-020-00348-w>, 2020.
- Petzold, A., Kramer, H., and Schönlinner, M.: Continuous measurement of atmospheric black carbon using a multi-angle absorption photometer, *Environ. Sci. Pollut. R. Special issue 4*, 78–82, 2002.
- 875 Petzold, A. and Schönlinner, M.: Multi-angle absorption photometry – A new method for the measurement of aerosol light absorption and atmospheric black carbon, *J. Aerosol Sci.*, 35, 421–441, <https://doi.org/10.1016/j.jaerosci.2003.09.005>, 2004. Petzold, A., Schloesser, H., Sheridan, P. J., Arnott, W. P., Ogren, J. A., and Virkkula, A.: Evaluation of multiangle absorption photometry for measuring aerosol light absorption, *Aerosol Sci. Tech.*, 39, 1, 40–51, 880 <https://doi.org/10.1080/027868290901945>, 2005.
- Petzold, A., Ogren, J. A., Fiebig, M., Laj, P., Li, S. M., Baltensperger, U., Holzer-Popp, T., Kinne, S., Pappalardo, G., Sugimoto, N., Wehrli, C., Wiedensohler, A., and Zhang, X.-Y.: Recommendations for reporting black carbon measurements, *Atmos. Chem. Phys.*, 13, 8365–8379, <https://doi.org/10.5194/acp-13-8365-2013>, 2013.
- 885 Pileci, R. E., Modini, R. L., Bertò, M., Yuan, J., Corbin, J. C., Marinoni, A., Henzing, B., Moerman, M. M., Putaud, J. P., Spindler, G., Wehner, B., Müller, T., Tuch, T., Trentini, A., Zanatta, M., Baltensperger, U., and Gysel-Beer, M.: Comparison of co-located refractory black carbon (rBC) and elemental carbon (EC) mass concentration measurements during field campaigns at several European sites, *Atmos. Meas. Tech.*, 14, 1379–1403, <https://doi.org/10.5194/amt-14-1379-2021>, 890 2021.
- Sand, M., Berntsen, T. K., Von Salzen, K., Flanner, M. G., Langner, J., and Victor, D. G.: Response of Arctic temperature to changes in emissions of short-lived climate forcers, *Nat. Clim. Change*, 6, 286–289, <https://doi.org/10.1038/nclimate2880>, 2016.
- Schmeisser, L., Andrews, E., Ogren, J. A., Sheridan, P., Jefferson, A., Sharma, S., Kim, J. E., Sherman, J. P., Sorribas, M., Kalapov, I., Arsov, T., Angelov, C., Mayol-Bracero, O. L., Labuschagne, C., 895 Kim, S.-W., Hoffer, A., Lin, N.-H., Chia, H.-P., Bergin, M., Sun, J., Liu, P., and Wu, H.: Classifying aerosol type using in situ surface spectral aerosol optical properties, *Atmos. Chem. Phys.*, 17, 12097–12120, <https://doi.org/10.5194/acp-17-12097-2017>, 2017.
- Schmeisser, L., Backman, J., Ogren, J. A., Andrews, E., Asmi, E., Starkweather, S., Uttal, T., Fiebig, 900 M., Sharma, S., Eleftheriadis, K., Vratolis, S., Bergin, M., Tunved, P., and Jefferson, A.:



- Seasonality of aerosol optical properties in the Arctic, *Atmos. Chem. Phys.*, 18, 11599–11622, <https://doi.org/10.5194/acp-18-11599-2018>, 2018.
- Schmid, H., Laskus, L., Jürgen Abraham, H., Baltensperger, U., Lavanchy, V., Bizjak, M., Burba, P., Cachier, H., Crow, D., Chow, J., Gnauk, T., Even, A., Ten Brink, H. M., Giesen, K. P.,  
905 Hitznerberger, R., Hueglin, C., Maenhaut, W., Pio, C., Carvalho, A., Putaud, J. P., Toom-Sauntry, D., and Puxbaum, H.: Results of the “carbon conference” international aerosol carbon round robin test stage I, *Atmos. Environ.*, 35, 2111–2121, [https://doi.org/10.1016/S1352-2310\(00\)00493-3](https://doi.org/10.1016/S1352-2310(00)00493-3), 2001.
- Schulz, H., Zanatta, M., Bozem, H., Richard Leaitch, W., Herber, A. B., Burkart, J., Willis, M. D.,  
910 Kunkel, D., Hoor, P. M., Abbatt, J. P. D., and Gerdes, R.: High Arctic aircraft measurements characterising black carbon vertical variability in spring and summer, *Atmos. Chem. Phys.*, 19, 2361–2384, <https://doi.org/10.5194/acp-19-2361-2019>, 2019.
- Schwarz, J. P., Gao, R. S., Fahey, D. W., Thomson, D. S., Watts, L. A., Wilson, J. C., Reeves, J. M., Darbeheshti, M., Baumgardner, D. G., Kok, G. L., Chung, S. H., Schulz, M., Hendricks, J., Lauer,  
915 A., Kärcher, B., Slowik, J. G., Rosenlof, K. H., Thompson, T. L., Langford, A. O., Loewenstein, M., and Aikin, K. C.: Single-particle measurements of midlatitude black carbon and light-scattering aerosols from the boundary layer to the lower stratosphere, *J. Geophys. Res. Atmos.*, 111, D16207, <https://doi.org/10.1029/2006JD007076>, 2006.
- Sharma, S., Lavoué, D., Chachier, H., Barrie, L. A. and Gong, S. L.: Long-term trends of the black  
920 carbon concentrations in the Canadian Arctic, *J. Geophys. Res.*, 109, D15203, <https://doi.org/10.1029/2003JD004331>, 2004.
- Sharma, S., Andrews, E., Barrie, L. A., Ogren, J. A., and Lavoué, D.: Variations and sources of the equivalent black carbon in the high Arctic revealed by long-term observations at Alert and Barrow: 1989–2003, *J. Geophys. Res.*, 111, D14028, <https://doi.org/10.1029/2005JD006581>,  
925 2006.
- Sharma, S., Leaitch, W. R., Huang, L., Veber, D., Kolonjari, F., Zhang, W., Hanna, S. J., Bertram, A. K., and Ogren, J. A.: An evaluation of three methods for measuring black carbon in Alert, Canada, *Atmos. Chem. Phys.*, 17, 15225–15243, <https://doi.org/10.5194/acp-17-15225-2017>, 2017.
- Sinha, P. R., Kondo, Y., Koike, M., Ogren, J. A., Jefferson, A., Barrett, T. E., Sheesley, R. J., Ohata, S.,  
930 Moteki, N., Coe, H., Liu, D., Irwin, M., Tunved, P., Quinn, P. K., and Zhao, Y.: Evaluation of ground-based black carbon measurements by filter-based photometers at two Arctic sites, *J. Geophys. Res. Atmos.*, 122, 3544–3572. <https://doi.org/10.1002/2016JD025843>, 2017.
- World Meteorological Organization/Global Atmosphere Watch: WMO/GAW aerosol measurement procedures, guidelines, and recommendations, GAW Report No. 227, 2016.



- 935 Yoshida, A., Moteki, N., Ohata, S., Mori, T., Tada, R., Dagsson-Waldhauserová, P., and Kondo, Y.:  
Detection of light-absorbing iron oxide particles using a modified single-particle soot photometer,  
Aerosol Sci. Tech., 50, 3, i–iv, <https://doi.org/10.1080/02786826.2016.1146402>, 2016.
- Yoshida, A., Ohata, S., Moteki, N., Adachi, K., Mori, T., Koike, M., and Takami, A.: Abundance and  
Emission Flux of the Anthropogenic Iron Oxide Aerosols From the East Asian Continental  
940 Outflow, J. Geophys. Res. Atmos., 123, 11, 194–11, 209, <https://doi.org/10.1029/2018JD028665>,  
2018.
- Yoshida, A., Moteki, N., Ohata, S., Mori, T., Koike, M., Kondo, Y., Matsui, H., Oshima, N., Takami,  
A., and Kita, K.: Abundances and Microphysical Properties of Light-Absorbing Iron Oxide and  
Black Carbon Aerosols Over East Asia and the Arctic, J. Geophys. Res. Atmos., 125,  
945 <https://doi.org/10.1029/2019JD032301>, 2020.
- Yuan, J., Modini, R. L., Zanatta, M., Herber, A. B., Müller, T., Wehner, B., Poulain, L., Tuch, T.,  
Baltensperger, U., and Gysel-beer, M.: Variability in the mass absorption cross section of black  
carbon (BC) aerosols is driven by BC internal mixing state at a central European background site  
(Melpitz, Germany) in winter, Atmos. Chem. Phys., 21, 635–655, [https://doi.org/10.5194/acp-21-](https://doi.org/10.5194/acp-21-635-2021)  
950 [635-2021](https://doi.org/10.5194/acp-21-635-2021), 2021.
- Zanatta, M., Gysel, M., Bukowiecki, N., Müller, T., Weingartner, E., Areskoug, H., Fiebig, M., Yttri, K.  
E., Mihalopoulos, N., Kouvarakis, G., Beddows, D., Harrison, R. M., Cavalli, F., Putaud, J. P.,  
Spindler, G., Wiedensohler, A., Alastuey, A., Pandolfi, M., Sellegri, K., Swietlicki, E., Jaffrezo, J.  
L., Baltensperger, U., and Laj, P.: A European aerosol phenomenology-5: Climatology of black  
955 carbon optical properties at 9 regional background sites across Europe, Atmos. Environ., 145,  
346–364, <https://doi.org/10.1016/j.atmosenv.2016.09.035>, 2016.
- Zanatta, M., Laj, P., Gysel, M., Baltensperger, U., Vratolis, S., Eleftheriadis, K., Kondo, Y., Dubuisson,  
P., Winiarek, V., Kazadzis, S., Tunved, P., and Jacobi, H.-W.: Effects of mixing state on optical  
and radiative properties of black carbon in the European Arctic, Atmos. Chem. Phys., 18, 14037–  
960 14057, <https://doi.org/10.5194/acp-18-14037-2018>, 2018.



## Figures

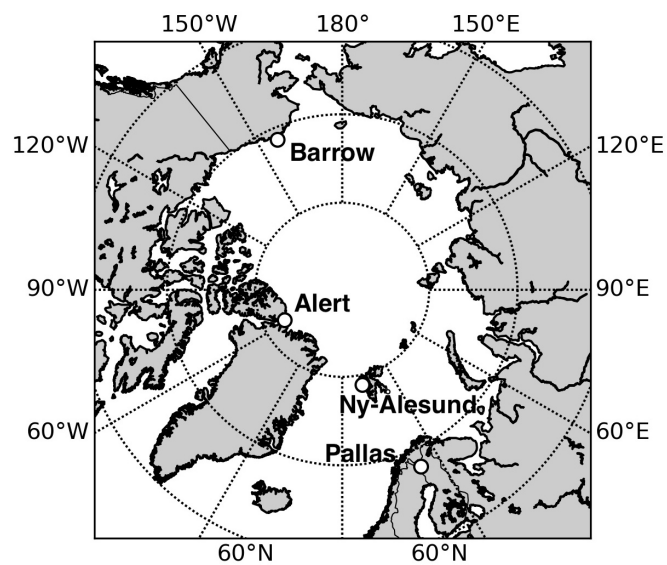


**Figure 1.** Locations of the Arctic sites where BC was measured for this study.

965

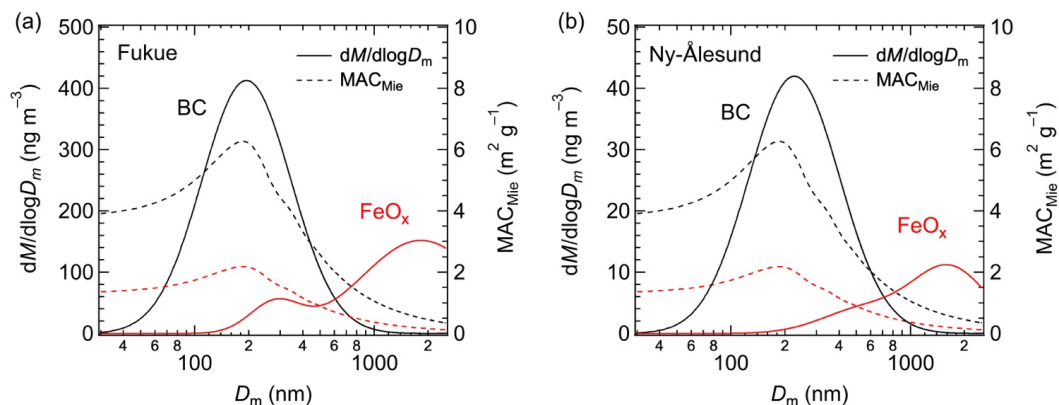
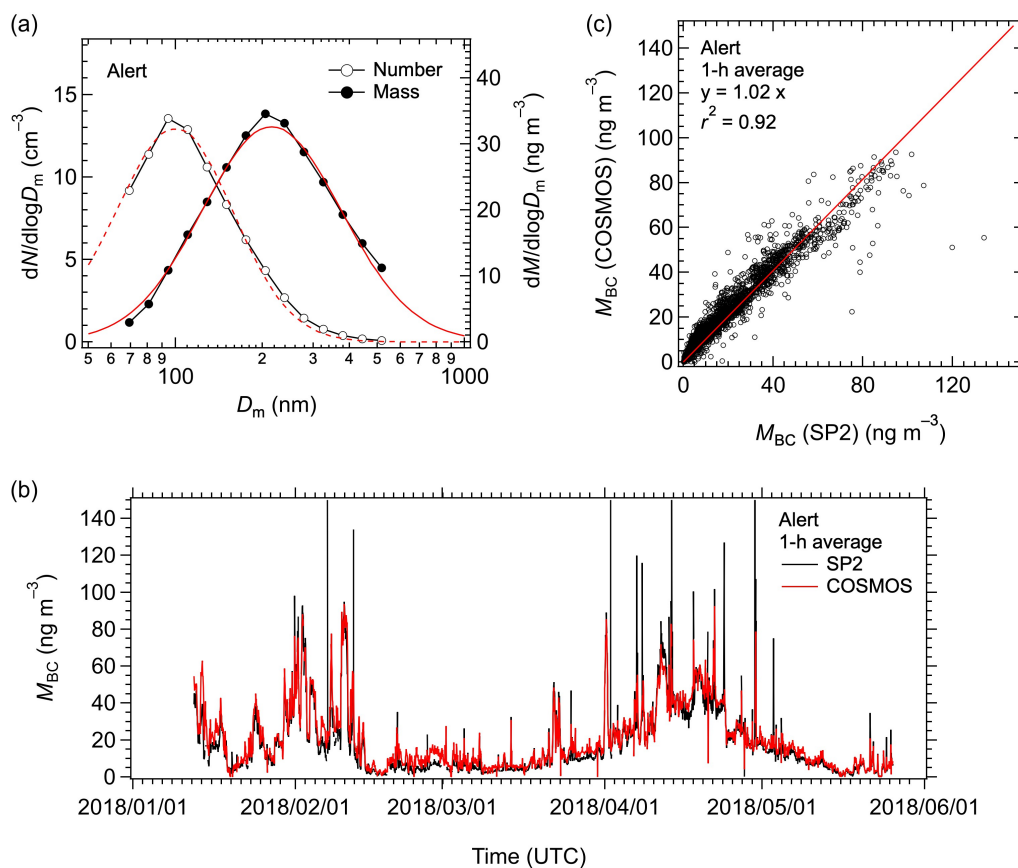


**Figure 2.** Mass size distributions of BC (black line) and  $\text{FeO}_x$  (red line) and mass absorption cross sections calculated by Mie theory for bare BC (black dashed line) and bare  $\text{FeO}_x$  (red dashed line) at (a) Fukue in April 2019 and (b) Ny-Ålesund in March 2017. Assumptions for the Mie calculations are

970 given in Sect. 2.



975 **Figure 3.** (a) Number and mass size distributions of BC averaged over the observation period at Alert from January to May 2018. The dashed (solid) red line is the lognormal fit to the number (mass) size distribution. (b) Time series (1-h data) and (c) correlation of  $M_{BC}$  measured by COSMOS and SP2. The solid line in the correlation plot is the least squares regression forced through the origin.

980



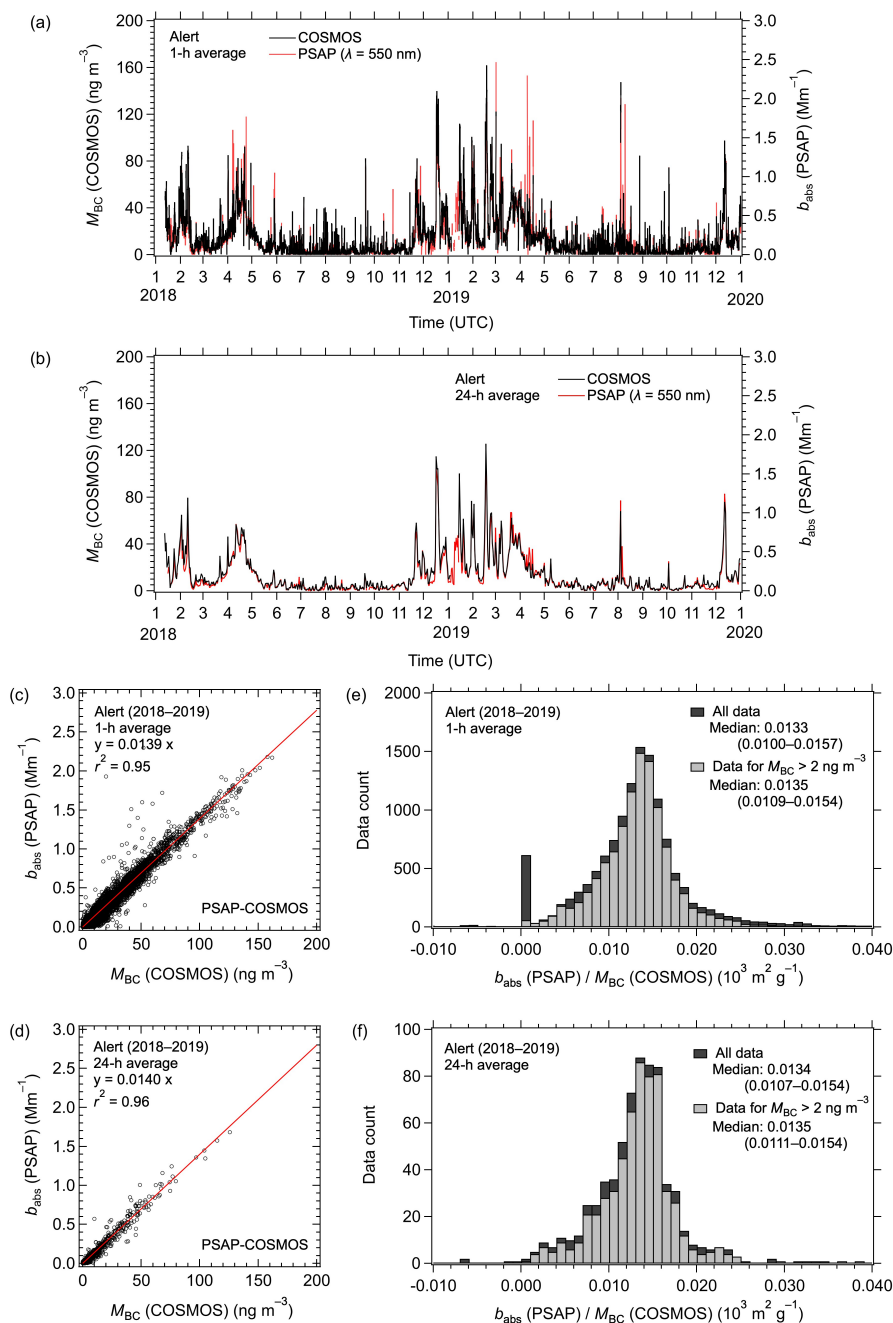


**Figure 4.** Time series of  $M_{BC}$  (COSMOS) and  $b_{abs}$  (PSAP;  $\lambda = 550 \text{ nm}$ ) from January 2018 to December 2019 at Alert for (a) 1-h averaged and (b) 24-h averaged data. (c) and (d) Corresponding correlations of  $M_{BC}$  (COSMOS) and  $b_{abs}$  (PSAP). The solid lines are the least squares regressions forced through the origin. (e) and (f) Corresponding histograms of  $b_{abs}$  (PSAP) /  $M_{BC}$  (COSMOS) ratios for all data and data with  $M_{BC}$  (COSMOS)  $> 2 \text{ ng m}^{-3}$ . The interquartile ranges are shown in parentheses.

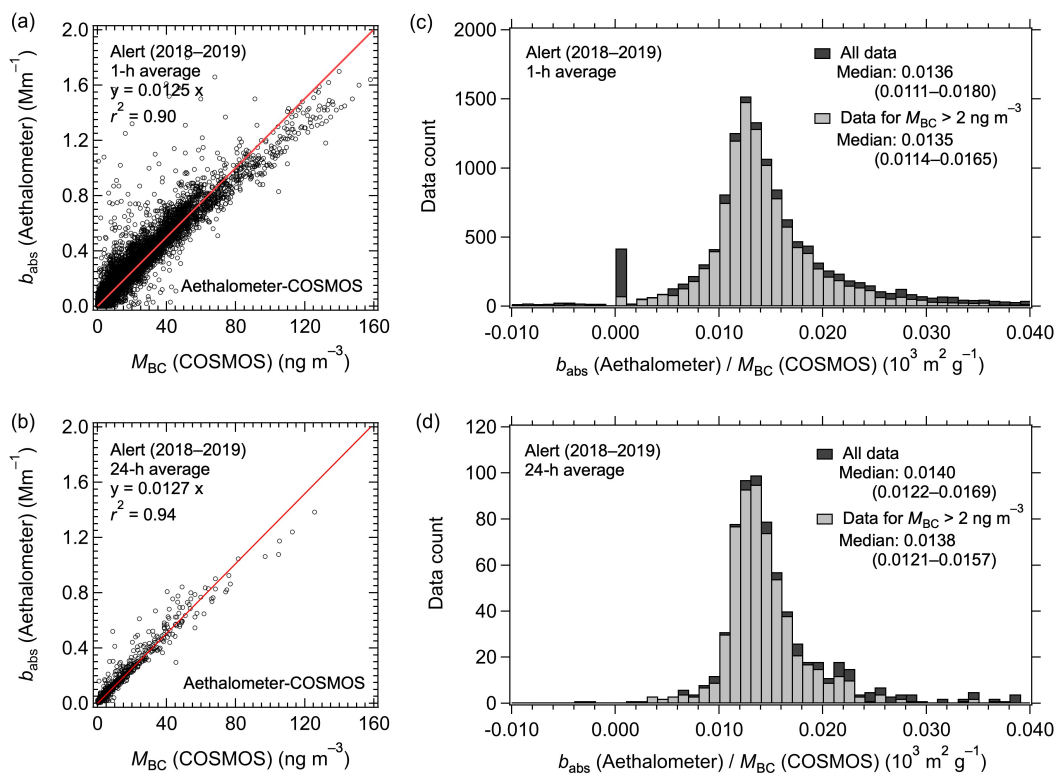
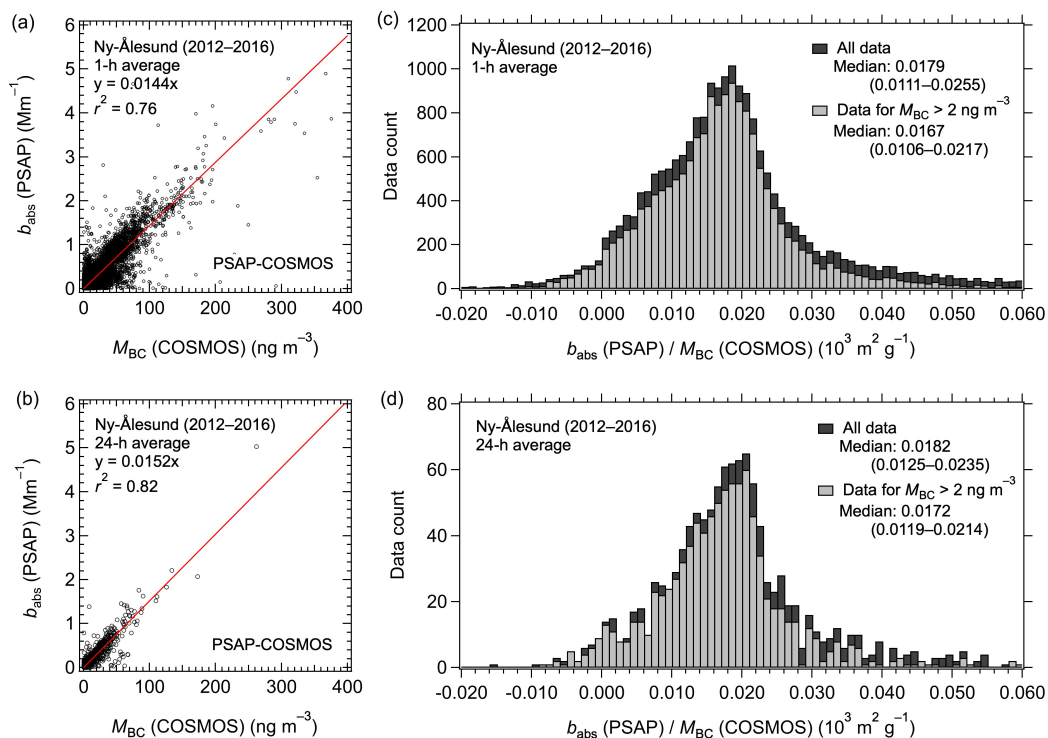


**Figure 5.** Correlations of  $M_{BC}$  (COSMOS) and  $b_{abs}$  (Aethalometer;  $\lambda = 590 \text{ nm}$ ) from January 2018 to December 2019 at Alert for (a) 1-h averaged and (b) 24-h averaged data. The solid lines are the least squares regressions forced through the origin. (c) and (d) Corresponding histograms of  $b_{abs}$  (Aethalometer) /  $M_{BC}$  (COSMOS) ratios for all data and data with  $M_{BC}$  (COSMOS)  $> 2 \text{ ng m}^{-3}$ .



995

**Figure 6.** Correlations of  $M_{BC}$  (COSMOS) and  $b_{abs}$  (PSAP;  $\lambda = 550 \text{ nm}$ ) from April 2012 to September 2016 at Ny-Ålesund for (a) 1-h averaged and (b) 24-h averaged data. The solid lines are the least squares regressions forced through the origin. (c) and (d) Corresponding histograms of  $b_{abs}$  (PSAP) /  $M_{BC}$  (COSMOS) ratios for all data and data with  $M_{BC}$  (COSMOS)  $> 2 \text{ ng m}^{-3}$ .

1000

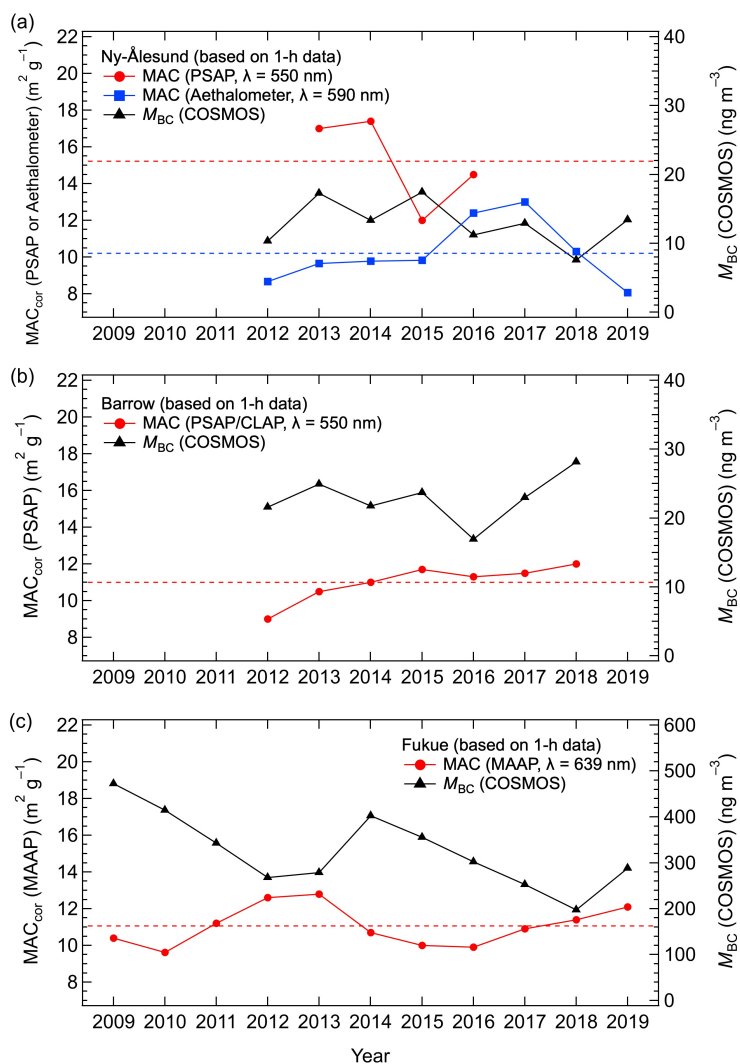
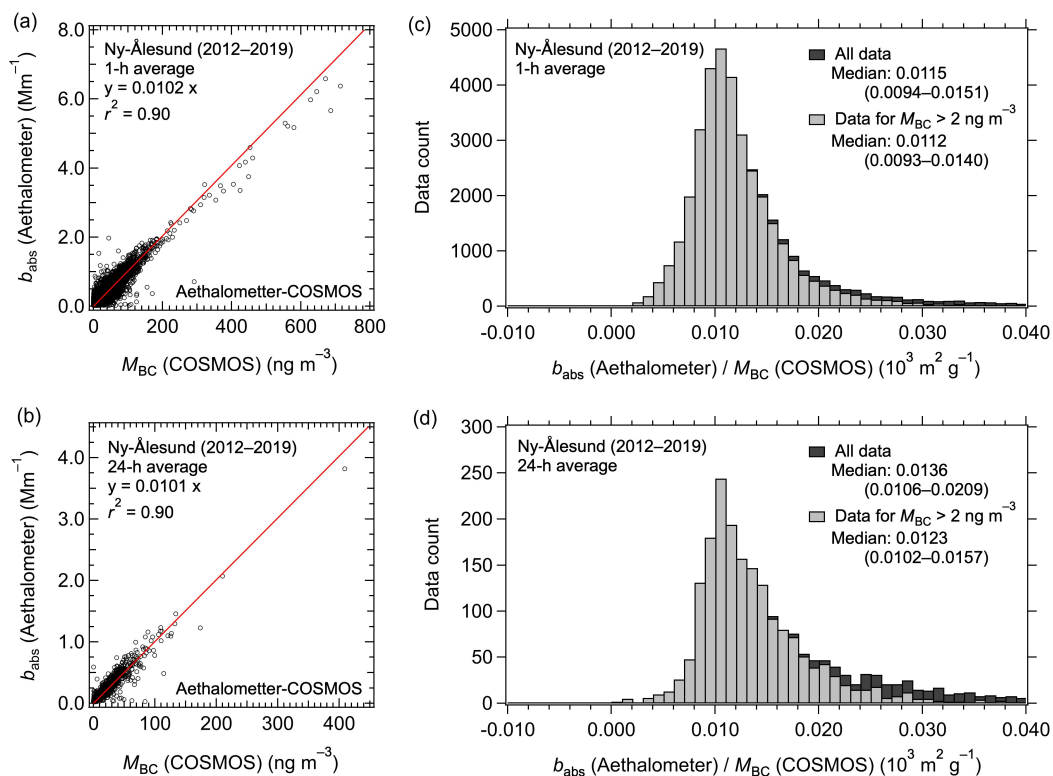


**Figure 7.** (a) Time series of yearly  $\text{MAC}_{\text{cor}}$  (PSAP;  $\lambda = 550$  nm),  $\text{MAC}_{\text{cor}}$  (Aethalometer;  $\lambda = 590$  nm), and  $M_{\text{BC}}$  (COSMOS) at Ny-Ålesund. (b) Time series of yearly  $\text{MAC}_{\text{cor}}$  (PSAP/CLAP;  $\lambda = 550$  nm) and  $M_{\text{BC}}$  (COSMOS) at Barrow. (c) Time series of yearly  $\text{MAC}_{\text{cor}}$  (MAAP;  $\lambda = 639$  nm) and  $M_{\text{BC}}$  (COSMOS) at Fukue. In each panel, yearly  $\text{MAC}_{\text{cor}}$  and  $M_{\text{BC}}$  (COSMOS) are calculated from 1-h data. The dashed lines show the averages of yearly  $\text{MAC}_{\text{cor}}$  for the entire time series.



1010

**Figure 8.** Correlations of  $M_{\text{BC}}$  (COSMOS) and  $b_{\text{abs}}$  (Aethalometer;  $\lambda = 590 \text{ nm}$ ) from April 2012 to August 2019 at Ny-Ålesund for (a) 1-h averaged and (b) 24-h averaged data. The solid lines are the least squares regressions forced through the origin. (c) and (d) Corresponding histograms of  $b_{\text{abs}}$  (Aethalometer) /  $M_{\text{BC}}$  (COSMOS) ratios for all data and data with  $M_{\text{BC}}$  (COSMOS)  $> 2 \text{ ng m}^{-3}$ .

1015

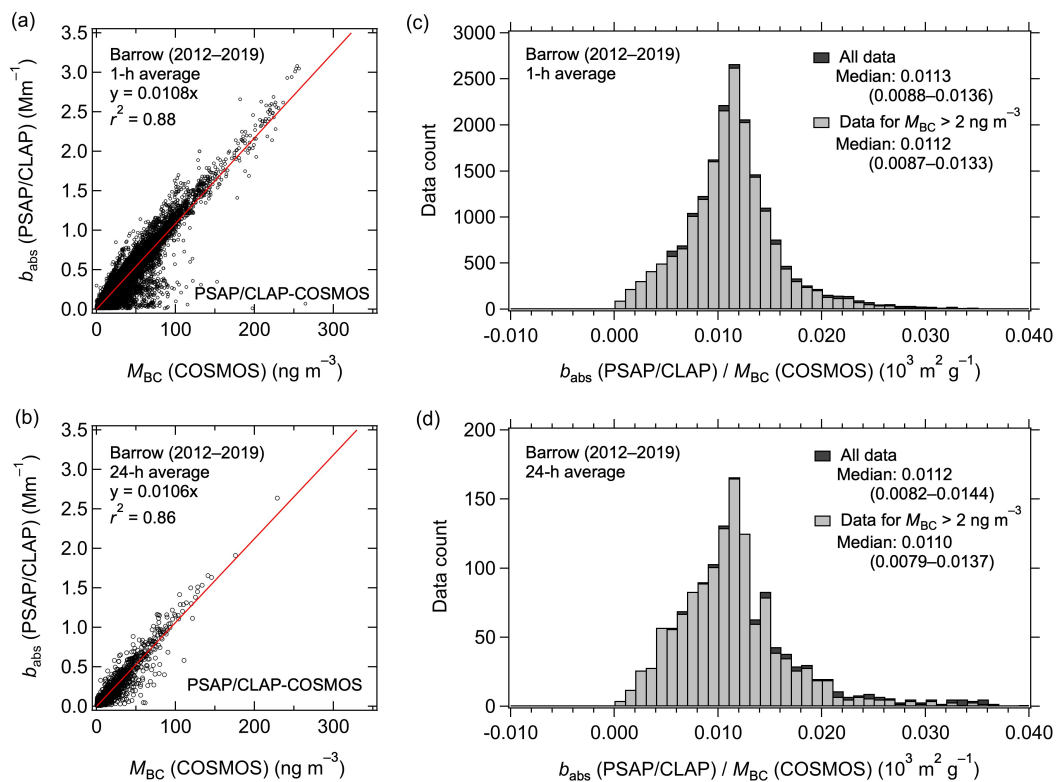
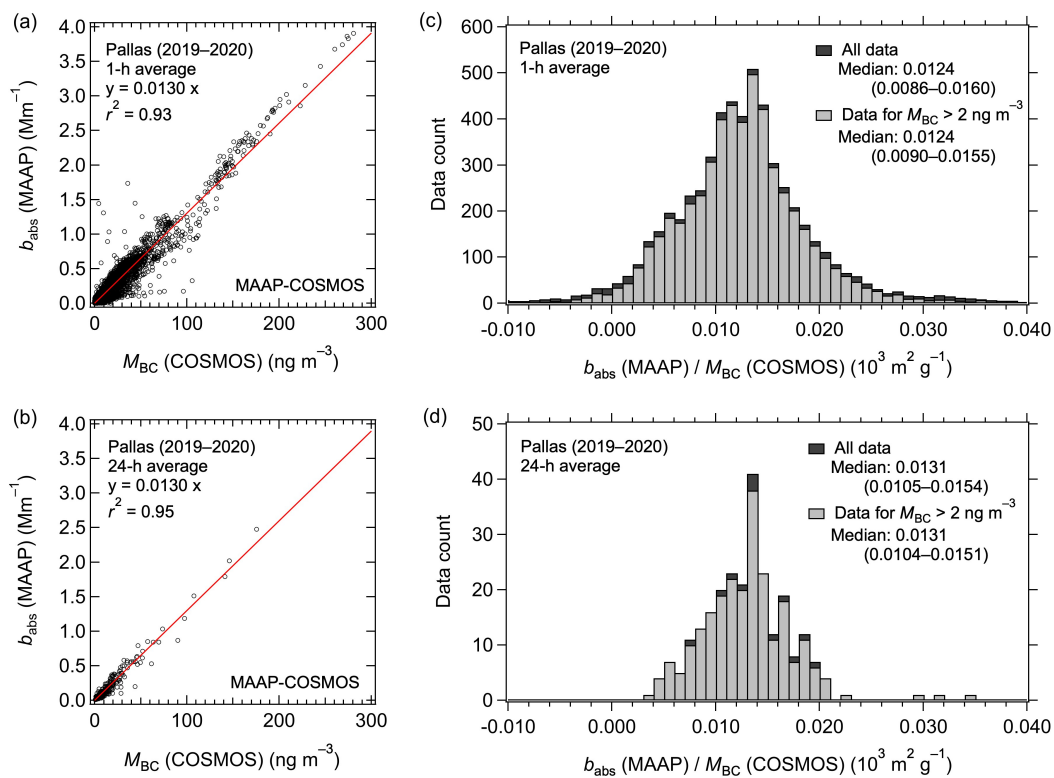


**Figure 9.** Correlations of  $M_{BC}$  (COSMOS) and  $b_{abs}$  (PSAP/CLAP;  $\lambda = 550$  nm) from August 2012 to December 2019 at Barrow for (a) 1-h averaged and (b) 24-h averaged data. The solid lines are the least squares regressions forced through the origin. (c) and (d) Corresponding histograms of  $b_{abs}$  (PSAP/CLAP) /  $M_{BC}$  (COSMOS) ratios for all data and data with  $M_{BC}$  (COSMOS)  $> 2\ ng\ m^{-3}$ .



1025 **Figure 10.** Correlations of  $M_{BC}$  (COSMOS) and  $b_{abs}$  (MAAP;  $\lambda = 637$  nm) from July 2019 to July 2020 at Pallas for (a) 1-h averaged and (b) 24-h averaged data. The solid lines are the least squares regressions forced through the origin. (c) and (d) Corresponding histograms of  $b_{abs}$  (MAAP) /  $M_{BC}$  (COSMOS) ratios for all data and data with  $M_{BC}$  (COSMOS)  $> 2$  ng m $^{-3}$ .

1030



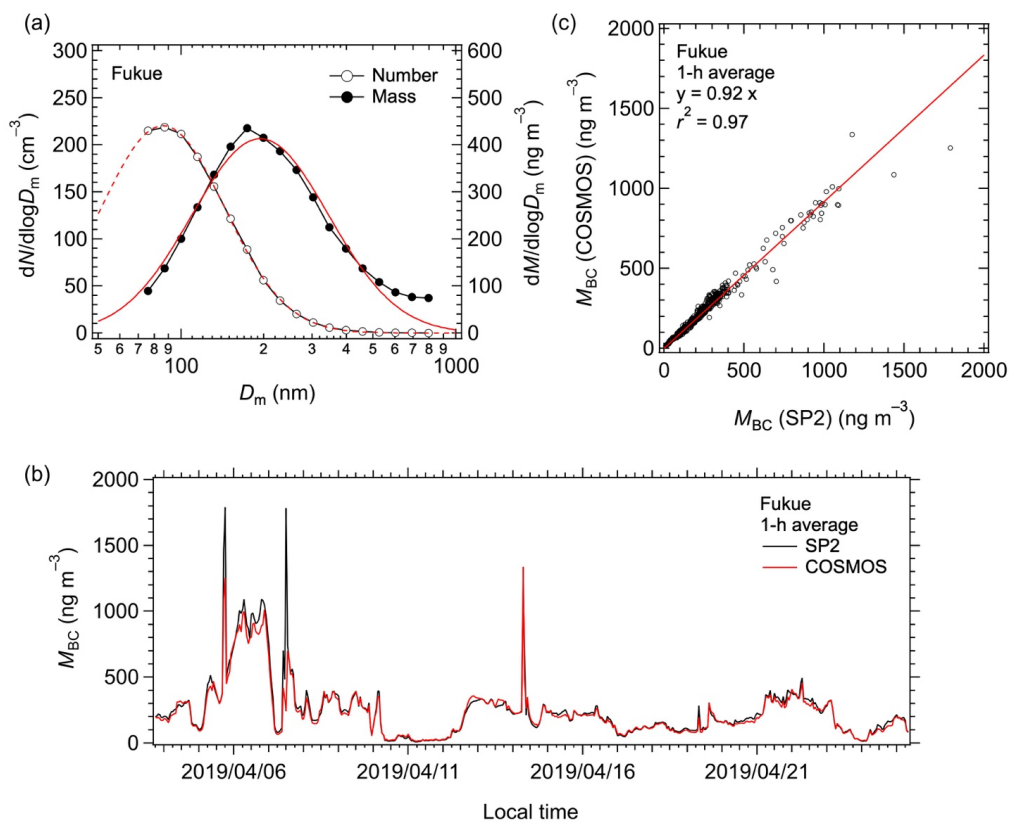


**Figure 11.** (a) Number and mass size distributions of BC averaged over the observation period at Fukue in April 2019. The dashed (solid) red line is the lognormal fit to the number (mass) size distribution. (b) Time series (1-h data) and (c) correlation of  $M_{\text{BC}}$  measured by COSMOS and SP2. The solid line in the correlation plot is the least squares regression forced through the origin.

1035

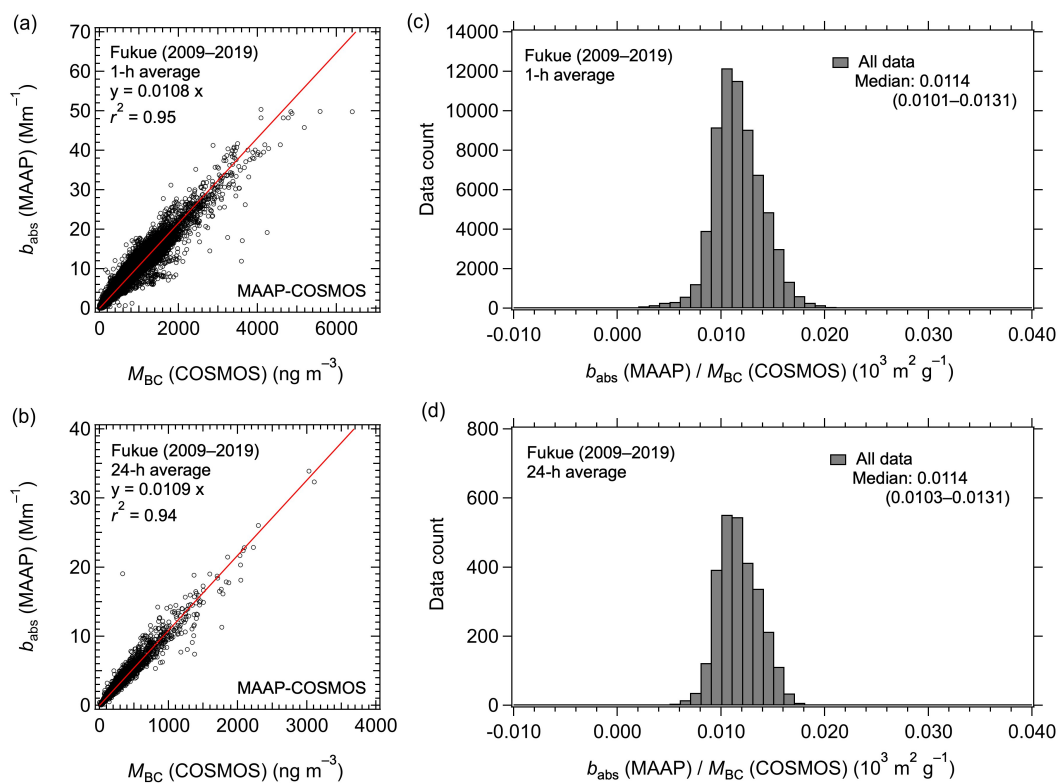


**Figure 12.** Correlations of  $M_{BC}$  (COSMOS) and  $b_{abs}$  (MAAP;  $\lambda = 639 \text{ nm}$ ) from April 2009 to May 1040 2019 at Fukue for (a) 1-h averaged and (b) 24-h averaged data. The solid lines are the least squares regression forced through the origin. (c) and (d) Corresponding histograms of  $b_{abs}$  (MAAP) /  $M_{BC}$  (COSMOS) ratios.

1045



## Tables

**Table 1.** Observation sites, periods, and instruments used in this study.

	Location	Period	Instruments
1050	Alert	Jan – May 2018	COSMOS, EC-SP2
		Jan 2018 – Dec 2019	COSMOS, PSAP, Aethalometer
	Ny-Ålesund	Apr 2012 – Sep 2016	COSMOS, PSAP
		Apr 2012 – Aug 2019	COSMOS, Aethalometer
	Barrow	Aug 2012 – Dec 2019	COSMOS, PSAP, CLAP
1055	Pallas	Jul 2019 – Jul 2020	COSMOS, MAAP
	Fukue (Japan)	Apr 2019	COSMOS, UT-SP2
		Apr 2009 – May 2019	COSMOS, MAAP

1060 **Table 2.**  $MAC_{cor}$  (PSAP/CLAP;  $\lambda$ ) values at Alert during 2018–2019.  $r^2$  is the square of the correlation coefficient.

1065	Instrument	$\lambda$ (nm)	$MAC_{cor}$ (1-h)		$MAC_{cor}$ (24-h)	
			$[m^2 g^{-1}]$	$r^2(1-h)$	$[m^2 g^{-1}]$	$r^2(24-h)$
	CLAP1	450	13.6	0.93	13.6	0.95
	CLAP2	450	15.4	0.96	15.4	0.96
	PSAP	450	15.7	0.95	15.4	0.96
	CLAP1	550	12.1	0.93	12.1	0.95
1070	CLAP2	550	13.6	0.96	13.8	0.95
	PSAP	550	13.9	0.96	14.0	0.95
	CLAP1	700	9.7	0.93	9.7	0.95
	CLAP2	700	10.8	0.95	10.9	0.95
	PSAP	700	11.5	0.94	11.6	0.95

1075



1080 **Table 3.** MAC,  $r^2$ , and variability of MAC of MAAP, PSAP/CLAP, and Aethalometer at observation sites in this study.

Loca tion	Instrument	Wave- length [nm]	Inlet	Period	(1-h)				(24-h)			
					MAC <sub>cor</sub> [m <sup>2</sup> g <sup>-1</sup> <sub>1</sub> ]	$r^2$	MAC <sub>med</sub> [m <sup>2</sup> g <sup>-1</sup> ]	$V_{MAC}$ [%]	MAC <sub>cor</sub> [m <sup>2</sup> g <sup>-1</sup> <sub>1</sub> ]	$r^2$	MAC <sub>med</sub> [m <sup>2</sup> g <sup>-1</sup> ]	$V_{MAC}$ [%]
Alert	PSAP	550	PM <sub>1</sub>	2018– 2019	13.9	0.95	13.5	19	14.0	0.96	13.5	18
Alert	Aethalo meter	590	TSP*	2018– 2019	12.5	0.90	13.5	22	12.7	0.94	13.8	22
Ny- Ålesund	PSAP	550	PM <sub>10</sub>	2012– 2016	14.4	0.76	16.7	37	15.2	0.82	17.2	31
Ny- Ålesund	Aethalo meter	590	PM <sub>10</sub>	2012– 2019	10.2	0.90	11.2	25	10.1	0.90	12.3	28
Barrow	PSAP/CLAP	550	PM <sub>1</sub>	2012– 2019	10.8	0.88	11.2	22	10.6	0.86	11.0	26
Pallas	MAAP	637	PM <sub>10</sub>	2019– 2020	13.0	0.93	12.4	27	13.0	0.95	13.1	21
Fukue	MAAP	639	PM <sub>1</sub> **	2009– 2019	10.8	0.95	11.4	15	10.9	0.94	11.4	15

\*Total suspended particle.

1085 \*\* A PM<sub>2.5</sub> cyclone was used before November 2011.

1090 **Table 4.** MAC<sub>cor</sub> (Aethalometer;  $\lambda$ ) and  $r^2$  values at Alert during 2018–2019.

	$\lambda$ (nm)	MAC <sub>cor</sub> (1-h)		MAC <sub>cor</sub> (24-h)	
		[m <sup>2</sup> g <sup>-1</sup> ]	$r^2$ (1-h)	[m <sup>2</sup> g <sup>-1</sup> ]	$r^2$ (24-h)
	370	18.6	0.86	18.7	0.90
1095	470	15.4	0.89	15.6	0.93
	520	13.9	0.90	14.1	0.94
	590	12.5	0.90	12.7	0.94
	660	11.4	0.89	11.6	0.94
	880	8.8	0.82	8.9	0.94
1100	950	8.1	0.79	8.1	0.94

1105



**Table 5.**  $MAC_{cor}$  (PSAP) and  $MAC_{cor}$  (Aethalometer) values derived from 24-h averaged data at Alert during 2018–2019.

$\lambda$ (nm)	$MAC_{cor}$ (PSAP)		$MAC_{cor}$ (Aeth)	
	PSAP/Aeth	$[m^2 g^{-1}]$	$[m^2 g^{-1}]$	$MAC_{cor} (Aeth) / MAC_{cor} (PSAP)$
450/470	15.4	15.6	1.01	(1.06)*
550/590	14.0	12.7	1.01	(1.03)*
700/660	11.6	11.6	1.00	(0.94)*

\*  $MAC_{cor}$  (Aethalometer) values measured at  $\lambda = 470, 590,$  and  $660$  nm were adjusted to those at  $\lambda = 450, 550,$  and  $700$  nm (wavelengths used for PSAP) by assuming an absorption Ångstrom exponent of 1.0.

**Table 6.** Year-to-year variability of  $MAC_{cor}$  (PSAP;  $\lambda = 550$  nm) and  $r^2$  at Ny-Ålesund.

Year	$MAC_{cor}$ (1-h)		$MAC_{cor}$ (24-h)	
	$[m^2 g^{-1}]$	$r^2$ (1-h)	$[m^2 g^{-1}]$	$r^2$ (24-h)
2012 (Apr–Dec)	5.7	0.30	5.8	0.44
2013	17.0	0.81	17.2	0.85
2014	17.4	0.80	18.5	0.81
2015	12.0	0.84	15.9	0.94
2016 (Jan–Sep)	14.5	0.90	14.8	0.95
Average (2013–2016)*	$15.2 \pm 2.2$	$0.84 \pm 0.04$	$16.6 \pm 1.4$	$0.89 \pm 0.06$
All**	14.4	0.76	15.2	0.82

\* Average and standard deviation for individual years

\*\* Derived by regression slope for all data points

**Table 7.** Year-to-year variability of  $MAC_{cor}$  (Aethalometer;  $\lambda = 590$  nm) and  $r^2$  at Ny-Ålesund.

Year	$MAC_{cor}$ (1-h)		$MAC_{cor}$ (24-h)	
	$[m^2 g^{-1}]$	$r^2$ (1-h)	$[m^2 g^{-1}]$	$r^2$ (24-h)
2012 (Apr–Dec)	8.67	0.80	8.75	0.85
2013	9.65	0.87	8.89	0.75
2014	9.77	0.92	10.0	0.95
2015	9.82	0.96	9.87	0.98
2016	12.4	0.92	12.2	0.95
2017	13.0	0.86	11.5	0.87
2018	10.3	0.92	10.6	0.94
2019 (Jan–Aug)	8.07	0.91	8.37	0.92
Average*	$10.2 \pm 1.6$	$0.90 \pm 0.05$	$10.0 \pm 1.3$	$0.90 \pm 0.07$
All**	10.2	0.90	10.1	0.90

\* Average and standard deviation for individual years

\*\* Derived by regression slope for of all data points



**Table 8.** Year-to-year variability of MAC<sub>cor</sub> (PSAP/CLAP;  $\lambda = 550$  nm) and  $r^2$  at Barrow.

1160

Year	MAC <sub>cor</sub> (1-h)		MAC <sub>cor</sub> (24-h)	
	[m <sup>2</sup> g <sup>-1</sup> ]	$r^2$ (1-h)	[m <sup>2</sup> g <sup>-1</sup> ]	$r^2$ (24-h)
2012 (Aug–Dec)	9.00	0.65	8.80	0.67
2013	10.5	0.91	10.5	0.91
1165 2014	11.0	0.96	10.8	0.91
2015	11.7	0.91	11.5	0.91
2016	11.3	0.89	11.2	0.88
2017	11.5	0.91	11.3	0.93
2018 (Jan–May)	12.0	0.86	10.9	0.69
1170 2019 (Jun–Dec)	4.6	0.28	5.1	0.41
Average (2012–2018)*	11.0 ± 0.9	0.87 ± 0.09	10.7 ± 0.8	0.84 ± 0.10
All**	10.8	0.88	10.6	0.86

\*Average and standard deviation for individual years

1175

\*\*Derived by regression slope for all data points

**Table 9.** Year-to-year variability of MAC<sub>cor</sub> (MAAP;  $\lambda = 639$  nm) and  $r^2$  at Fukue.

1180

Year	MAC <sub>cor</sub> (1-h)		MAC <sub>cor</sub> (24-h)	
	[m <sup>2</sup> g <sup>-1</sup> ]	$r^2$ (1-h)	[m <sup>2</sup> g <sup>-1</sup> ]	$r^2$ (24-h)
2009 (Apr–Dec)	10.4	0.98	10.5	0.99
2010	9.62	0.95	9.74	0.95
1185 2011	11.2	0.95	11.3	0.96
2012	12.6	0.96	12.7	0.96
2013	12.8	0.94	12.7	0.94
2014	10.7	0.98	10.8	0.98
2015	10.0	0.96	9.96	0.95
1190 2016	9.90	0.95	9.97	0.95
2017	10.9	0.93	11.1	0.90
2018	11.4	0.96	11.5	0.96
2019 (Jan–May)	12.1	0.95	12.2	0.95
Average*	11.1 ± 1.0	0.96 ± 0.01	11.1 ± 1.0	0.95 ± 0.02
1195 All**	10.8	0.95	10.9	0.94

\*Average and standard deviation for individual years

\*\*Derived by regression slope for all data points

1200



1205

**Table 10.**  $MAC_{cor}$  and  $r^2$  for MAAP, PSAP/CLAP, and Aethalometer at  $\lambda = 550$  nm at observation sites in this study.

Location	Instrument	Inlet	Period	(1-h)	$r^2$	(24-h)	$r^2$
				$MAC_{cor}$ [ $m^2 g^{-1}$ ]		$MAC_{cor}$ [ $m^2 g^{-1}$ ]	
Alert	PSAP	PM <sub>1</sub>	2018–2019	13.9	0.95	14.0	0.96
Alert	Aethalometer	TSP*	2018–2019	13.4***	0.89	13.6***	0.92
Ny-Ålesund	PSAP	PM <sub>10</sub>	2013–2016	14.4	0.76	15.2	0.82
Ny-Ålesund	Aethalometer	PM <sub>10</sub>	2012–2019	10.9***	0.90	10.8***	0.90
Barrow	PSAP/CLAP	PM <sub>1</sub>	2012–2018	10.8	0.88	10.6	0.86
Pallas	MAAP	PM <sub>10</sub>	2019–2020	15.1***	0.93	15.1***	0.95
Fukue	MAAP	PM <sub>1</sub> **	2009–2019	12.5***	0.95	12.7***	0.95
Average in the 4 Arctic sites****				13.1±1.7	0.89±0.06	13.2±1.9	0.91±0.05

\*Total suspended particles.

1210 \*\*A PM<sub>2.5</sub> cyclone was used before November 2011.

\*\*\*  $MAC_{cor}$  (MAAP;  $\lambda \sim 637$  nm) and  $MAC_{cor}$  (Aethalometer;  $\lambda = 590$  nm) values were adjusted to those at  $\lambda = 550$  nm by assuming an absorption Ångstrom exponent of 1.0.

\*\*\*\* Average and standard deviation values were calculated excluding MAAP data at Fukue.

1215